

University of Windsor

## Scholarship at UWindor

---

Electronic Theses and Dissertations

Theses, Dissertations, and Major Papers

---

1-1-2006

### Electrical transients in permanent magnet synchronous machines.

Shahram Najafi  
*University of Windsor*

Follow this and additional works at: <https://scholar.uwindsor.ca/etd>

---

#### Recommended Citation

Najafi, Shahram, "Electrical transients in permanent magnet synchronous machines." (2006). *Electronic Theses and Dissertations*. 7090.  
<https://scholar.uwindsor.ca/etd/7090>

This online database contains the full-text of PhD dissertations and Masters' theses of University of Windsor students from 1954 forward. These documents are made available for personal study and research purposes only, in accordance with the Canadian Copyright Act and the Creative Commons license—CC BY-NC-ND (Attribution, Non-Commercial, No Derivative Works). Under this license, works must always be attributed to the copyright holder (original author), cannot be used for any commercial purposes, and may not be altered. Any other use would require the permission of the copyright holder. Students may inquire about withdrawing their dissertation and/or thesis from this database. For additional inquiries, please contact the repository administrator via email ([scholarship@uwindsor.ca](mailto:scholarship@uwindsor.ca)) or by telephone at 519-253-3000ext. 3208.

**ELECTRICAL TRANSIENTS IN PERMANENT MAGNET  
SYNCHRONOUS MACHINES**

by

**Shahram Najafi**

**A Thesis**

**Submitted to the Faculty of Graduate Studies and Research  
through Electrical and Computer Engineering  
in Partial Fulfillment of the Requirements for the  
Degree of Master of Applied Science at the  
University of Windsor**

**Windsor, Ontario, Canada**

**2006**

**© 2006 Shahram Najafi**



Library and  
Archives Canada

Bibliothèque et  
Archives Canada

Published Heritage  
Branch

Direction du  
Patrimoine de l'édition

395 Wellington Street  
Ottawa ON K1A 0N4  
Canada

395, rue Wellington  
Ottawa ON K1A 0N4  
Canada

*Your file* *Votre référence*  
*ISBN: 978-0-494-35951-8*  
*Our file* *Notre référence*  
*ISBN: 978-0-494-35951-8*

**NOTICE:**

The author has granted a non-exclusive license allowing Library and Archives Canada to reproduce, publish, archive, preserve, conserve, communicate to the public by telecommunication or on the Internet, loan, distribute and sell theses worldwide, for commercial or non-commercial purposes, in microform, paper, electronic and/or any other formats.

The author retains copyright ownership and moral rights in this thesis. Neither the thesis nor substantial extracts from it may be printed or otherwise reproduced without the author's permission.

**AVIS:**

L'auteur a accordé une licence non exclusive permettant à la Bibliothèque et Archives Canada de reproduire, publier, archiver, sauvegarder, conserver, transmettre au public par télécommunication ou par l'Internet, prêter, distribuer et vendre des thèses partout dans le monde, à des fins commerciales ou autres, sur support microforme, papier, électronique et/ou autres formats.

L'auteur conserve la propriété du droit d'auteur et des droits moraux qui protègent cette thèse. Ni la thèse ni des extraits substantiels de celle-ci ne doivent être imprimés ou autrement reproduits sans son autorisation.

---

In compliance with the Canadian Privacy Act some supporting forms may have been removed from this thesis.

Conformément à la loi canadienne sur la protection de la vie privée, quelques formulaires secondaires ont été enlevés de cette thèse.

While these forms may be included in the document page count, their removal does not represent any loss of content from the thesis.

Bien que ces formulaires aient inclus dans la pagination, il n'y aura aucun contenu manquant.

  
**Canada**

## ABSTRACT

When permanent magnet synchronous machines are subjected to short-circuit, voltage sags, or voltage swells at their terminals, the accurate calculation of the machine transient performance depends on the short-circuit, voltage sag, or voltage swell profile and the saturation condition of their main flux paths. In this research work, computer models for permanent magnet synchronous machines have been developed using the machine flux and current differential equations considering saturation. A voltage profile due to fault at the machine terminal is proposed. The machine terminal voltage takes a certain period of time to fall to final fault value and preceding the fault clearing, to recover to final post-fault value. The effect of the main flux saturation both in the direct and quadrature axes on the determination of the transient performance of permanent magnet synchronous machines employing the proposed voltage profile is demonstrated in this research work.

## **DEDICATION**

This thesis is dedicated to my parents, wife, kids, who prayed for me, stood beside me facing all difficulties, and supported me throughout the course of this thesis. I would like to give special thanks to my mother who always urged me throughout my study. And to my wife who accepted difficulties and helped me a lot in my responsibilities and prepared a better atmosphere for my study.

## **ACKNOWLEDGEMENTS**

I wish to take the opportunity to thank my supervisor Dr. N. Kar for his technical guidance, supportive advice and his understanding to some of the difficulties I went through. Sincere thanks to my departmental reader Dr. R. Hackam for his helpful comments and suggestions to my thesis and for reviewing my thesis. My thanks are also extended to Dr. R. Seth for taking the time to review my work and participate in my examination committee. I would like to also thank my fellow graduate student for their support, helpful criticism and suggestions.

## TABLE OF CONTENTS

ABSTRACT	iii
DEDICATION	iv
ACKNOWLEDGEMENTS	v
LIST OF TABLES	viii
LIST OF FIGURES	ix
LIST OF SYMBOLS	xiv
CHAPTER	
1 INTRODUCTION	1
1.1 Background	1
1.1.1 Permanent Magnet Synchronous Machine Review	1
1.1.2 Existing Models of Permanent Magnet Synchronous Machine	3
1.1.3 Saturation	4
1.1.4 Electrical Transients	5
1.1.5 Voltage Profile	12
1.2 Objective	13
1.3 Scope	13
2 PROBLEM DEFINITION	16
2.1 Modeling of Permanent Magnet Synchronous Machines	16
2.2 Saturation	17
2.3 Electrical Transients	18
2.4 Voltage Profile	19
3 PMSM Modeling for Electrical Transient Analysis	21
3.1 Equivalent Circuits	21
3.2 Unsaturated Model	23
3.2.1 Model Using Flux Differential Equations	23
3.2.2 Model Using Current Differential Equations	24
3.3 Saturated Machine Models	26
3.3.1 Model Considering only q-Axis Saturation	26

3.3.2 Saturated Model Considering both d- & q-Axis Saturation	26
4 Numerical Investigation	28
4.1 System Studied and Machine Parameters	28
4.1.1 Machine Parameters	28
4.1.2 Machine Saturation Characteristics	30
4.2 Simulation Flowcharts	30
4.2.1 Procedures of Simulation	30
4.3 Numerical Calculation	39
4.3.1 Comparison of the Results Calculated by Methods 1 and 2	39
4.3.2 Short-Circuit Analysis	47
4.3.3 Voltage Sag Analysis	49
4.3.4 Voltage Swell Analysis	56
4.3.5 Voltage Profile Analysis	62
5 CONCLUSION	67
REFERENCES	69
VITA AUCTORIS	75



## **LIST OF TABLES**

<b>Table 1:</b>	<b>Machine Parameters</b>	<b>29</b>
<b>Table 2:</b>	<b>Operating Conditions</b>	<b>29</b>

## LIST OF FIGURES

Fig. 1	d-q model of permanent magnet synchronous machine	2
Fig. 2	Lightning stroke current that can result in impulsive transients on the power system [29]	6
Fig. 3	Oscillatory transient caused by back-to-back capacitor switching [29]	6
Fig. 4	Instantaneous voltage sag caused by a SLG fault [29]	7
Fig. 5	Momentary interruption due to a fault and subsequent recloser operation [29]	7
Fig. 6	Temporary voltage sag caused by motor starting [29]	8
Fig. 7	Voltage sag in one phase for duration of 50 ms	10
Fig. 8	Voltage swell in one phase for duration of 50 ms	12
Fig. 9	Numerous voltage profiles to represent the occurrence and clearing of a short-circuit fault	20
Fig. 10	d- and q-axis equivalent circuits	21
Fig. 11	Machine phasor diagram	22
Fig. 12	Single line diagram for the system studied	28
Fig. 13	d- and q-axis linear and open circuit characteristic curves	30
Fig. 14	Initial value calculation for the unsaturated model (methods 1 and 2 in model 1)	31
Fig. 15	Calculation of transient values using flux differential equations (method 1)	33
Fig. 16	Calculation of transient values using current differential equations (method 2)	34

Fig. 17	Initial values calculation for models considering saturation (cont'd)	35
Fig. 17	Initial values calculation for models considering saturation	36
Fig. 18	Transient value calculation using flux differential equations using saturated model (cont'd)	37
Fig. 18	Transient value calculation using flux differential equations using saturated model	38
Fig. 19	Electromagnetic torque for motor under lagging power factor condition and short-circuit duration of 41.67ms	40
Fig. 20	Electromagnetic torque for motor under leading power factor conditions and short-circuit duration of 41.67 ms	41
Fig. 21	Electromagnetic torque for generator under lagging power factor conditions and short-circuit duration of 41.67ms	41
Fig. 22	Electromagnetic torque for generator under leading power factor conditions and short-circuit duration of 41.67 ms	42
Fig. 23	d- and q-axis stator currents for motor under lagging power factor conditions and short-circuit duration of 41.67 ms	43
Fig. 24	d- and q-axis damper winding currents for motor under lagging power factor conditions and short-circuit duration of 41.67 ms	43
Fig. 25	d- and q-axis stator currents for motor under leading power factor conditions and short-circuit duration of 41.67 ms	44
Fig. 26	d- and q-axis damper winding currents for motor under leading power factor conditions and short-circuit duration of 41.67 ms	44
Fig. 27	d- and q-axis stator currents for generator under lagging power factor conditions and short-circuit duration of 41.67 ms	45

Fig. 28	d- and q-axis damper winding currents for generator under lagging power factor conditions and short-circuit duration of 41.67 ms	45
Fig. 29	d- and q-axis stator currents for generator under leading power factor conditions and short-circuit duration of 41.67 ms	46
Fig. 30	d- and q-axis damper winding currents for generator under leading power factor conditions and short-circuit duration of 41.67 ms	46
Fig. 31	Air-gap torque by the three saturation models under lagging power condition for short-circuit duration of 33.33 ms and voltage fall/recovery duration of 2.5 ms	48
Fig. 32	Phase 'a' current by the three saturation models under lagging power condition for short-circuit duration of 33.33 ms and voltage fall/recovery duration of 2.5 ms	48
Fig. 33	Load angle by the three saturation models under lagging power condition for short-circuit duration of 33.33 ms and voltage fall/recovery duration of 2.5 ms	49
Fig. 34	Motor air-gap torque calculated by various models under lagging power factor condition for sag duration of 28.33 ms	51
Fig. 35	Motor air-gap torque calculated by various models under lagging power factor condition for sag duration of 38.33 ms	51
Fig. 36	Peak torque vs sag magnitude calculated by the various models under lagging power factor condition for sag duration of 38.33 ms	52
Fig. 37	Motor phase 'a' current calculated by various models under lagging power factor condition for sag duration of 28.33 ms	53

Fig. 38	Motor phase 'a' current calculated by various models under lagging power factor condition for sag duration of 38.33 ms	53
Fig. 39	Motor peak phase 'a' current vs sag duration calculated by the various models under lagging power factor condition for sag duration of 38.33 ms	54
Fig. 40	Motor Load Angle calculated by various models under lagging power factor condition for sag duration of 28.33 ms	55
Fig. 41	Motor Load Angle calculated by various models under lagging power factor condition for sag duration of 38.33 ms	55
Fig. 42	Motor air-gap torque calculated by the various models under lagging power factor condition for voltage swell duration of 28.33 ms	57
Fig. 43	Motor air-gap torque calculated by the various models under lagging power factor condition for voltage swell duration of 38.33 ms	58
Fig. 44	Largest positive peak value of the post-swell air-gap torque vs swell magnitude calculated by the various models under lagging power factor condition for voltage swell duration of 38.33 ms	58
Fig. 45	Motor phase 'a' current calculated by the various models under lagging power factor condition for voltage swell duration of 28.33 ms	59
Fig. 46	Motor phase 'a' current calculated by the various models under lagging power factor condition for voltage swell duration of 38.33 ms	60
Fig. 47	Largest negative peak value of the post-swell phase 'a' current as a function of the swell magnitude calculated by the various models under lagging power factor condition for voltage swell duration of 28.33 ms	60

- Fig. 48 Motor load angle calculated by the various models under lagging 61  
power factor condition for voltage swell duration of 28.33 ms
- Fig. 49 Motor load angle calculated by the various models under lagging 62  
power factor condition for voltage swell duration of 38.33 ms
- Fig. 50 Proposed voltage profile due to short-circuit at the motor terminals 63  
with different voltage fall and recovery durations
- Fig. 51 Air-gap torque calculated using model considering both d- and q-axis 65  
saturation for short-circuit duration of 33.33 ms and using voltage fall  
and recovery duration of 0, 1.25, 2.5, 3.75 and 5 ms each
- Fig. 52 Phase 'a' current calculated using model considering both d- and q- 65  
axis saturation for short-circuit duration of 33.33 ms and using voltage  
fall and recovery duration of 0, 1.25, 2.5, 3.75 and 5 ms each
- Fig. 53 Load angle calculated using the three saturation models for short- 66  
circuit duration of 33.33 ms and using voltage fall and recovery  
duration of 0, 1.25, 2.5, 3.75 and 5 ms each
- Fig. 54 Motor critical clearing time as a function of voltage fall/recovery 66  
duration calculated by the three saturation models duration calculated  
by the three saturation models

## LIST OF SYMBOLS

$V_t$	:Terminal voltage
$I_t$	:Terminal current
$P_t$	:Terminal real power
$V_d, V_q$	:d- and q-axis components of the stator voltage
$V_{kd1}, V_{kq1}$	:d- and q-axis rotor damper winding voltages
$E_{pm}$	:Equivalent permanent magnet voltage
$i_d, i_q$	:d- and q-axis components of the stator current
$i_{kd1}, i_{kq1}$	:d- and q-axis rotor damper winding currents
$i_{md}, i_{mq}$	:d- and q-axis components of the magnetizing current
$i_{pm}$	:Equivalent permanent magnet current
$\Psi_d, \Psi_q$	:d- and q-axis components of the stator flux linkage
$\Psi_{kd1}, \Psi_{kq1}$	:d- and q-axis damper winding flux linkages
$\Psi_{pm}$	:Permanent magnet flux
$\Psi_{md}, \Psi_{mq}$	:d- and q-axis components of the magnetizing flux linkage
$AT_d, AT_q$	:d- and q-axis amperes-turns
$R$	:Stator winding resistance
$R_{kd1}, R_{kq1}$	:d- and q-axis rotor damper winding resistances
$X_d, X_q$	:d- and q-axis synchronous reactances
$X_{kd1}, X_{kq1}$	:d- and q-axis damper winding reactances
$X_{mds}, X_{mqs}$	:d- and q-axis saturated magnetizing reactances
$X_{mdu}, X_{mqu}$	:d- and q-axis unsaturated magnetizing reactances
$X_{ll}$	:Stator leakage reactance

$K_d, K_q$	:d- and q-axis saturation factors
$T_e$	:Electromagnetic air-gap torque
$\omega_s$	:Synchronous speed in rad/sec
$\omega_r$	:Rotor mechanical speed
$J$	:Moment of inertia of the rotor
$PF$	:Power factor
$\delta$	:Load angle
$\theta$	:Power factor angle
$V_B$	:Infinite bus voltage
$t$	:Time
$\Delta t$	:Time step
$n$	:Time counter
$t_n, t_{n+1}$	:Present and next time step
$k, k+1$	:Present and next iteration counter



# **1. INTRODUCTION**

## **1.1 Background**

### **1.1.1 Permanent Magnet Synchronous Machine Review**

Permanent magnet synchronous machines (PMSM) have attracted increasing interest in recent years and are being used increasingly in a wide range of industrial drives and servo applications [1]. The main advantages of permanent magnet synchronous machines over other machines [2]-[6] are as follows:

- There are no brushes and slip rings
- The absence of rotor excitation windings eliminates the field winding copper loss
- More efficient
- Posses higher power density
- Smaller frame size
- Higher torque to inertia ratio
- Lower rotor inertia for a given output.

The disadvantages of the permanent magnet synchronous machines [7] are:

- The higher costs of material and manufacture of their rotor
- Higher cost of maintenance
- Possible loss of permanent magnet magnetization
- Thermal limitation
- There is no control over the permanent magnet flux which leads to less flexibility.

However, developments in rare earth based permanent magnets are continually leading to both reduced material cost and higher stored energy characteristics and, thus, reducing the amount of material required. In this thesis, only interior permanent magnet synchronous machines which have the permanent magnets buried inside the rotor are considered. The interior magnet design offers the advantages of mechanical robustness and a smaller air gap [8]-[10]. The standard two-axis (d- and q-axis) theory with fixed rotor reference frame will be used, since when viewing the machine from the d- and q-axis fixed on the rotor, the reluctances along the direct and quadrature axes are constant regardless of the rotor position. The machine quantities in the abc reference frame can be converted into d- and q-axis quantities by using the Park's transformation [11], [12]. The d-q model of permanent magnet synchronous machine is shown in Fig. 1.

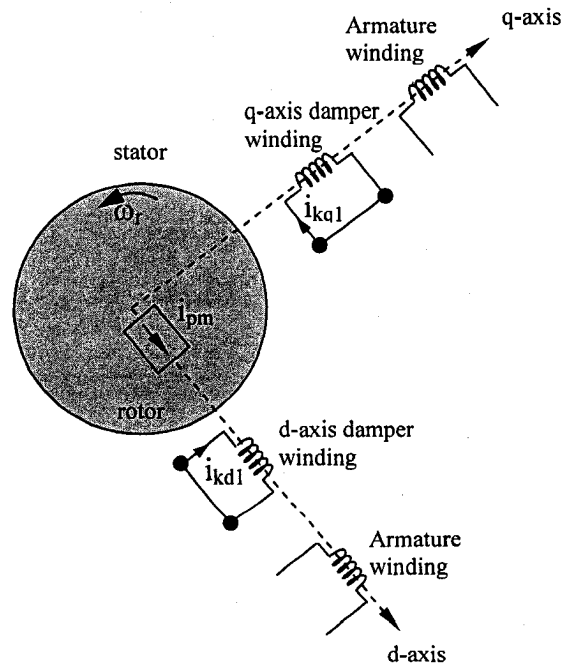


Fig. 1. d-q model of permanent magnet synchronous machine.

Damper windings can be added to the rotor of the machine to increase performance and dampen out speed oscillations, as well as aid in starting. However, damper winding effects (because of the induced eddy current in the rotor [13]) can still be present in a permanent magnet synchronous machine that does not have physical damper windings.

### **1.1.2 Existing Models of Permanent Magnet Synchronous Machines**

The wide field of applications of the permanent magnet synchronous machine includes those areas where dynamic performance is critical. In such cases, it is important to model the machine behavior to sufficient accuracy [14]. So, it is essential to predict synchronous and dynamic performances of a permanent magnet synchronous machine in order to avoid the design misjudgment that can prove costly once the motor is manufactured and to have better understanding of the permanent magnet synchronous machine dynamic performance [8].

Various mathematical models are available to describe the transient behavior of permanent magnet synchronous machines. Although they may differ in degree of complexity and accuracy, most of them are based on the well known two-axis (d- and q-axis) theory, and are solved by numerical integration. But modeling of permanent magnet synchronous machines presents difficulties due to permanent magnet excitation and machine's magnetic parameter variations due to saturation. Since there is no unified method of modeling permanent magnet synchronous machines, some researchers in the machine modeling ignore the need and effect of damper winding [15] and some researchers consider damper winding in the rotor [16]. In [17] iron and core losses are neglected, while in [18], iron and core losses are incorporated. Some researchers ignore

the effect of cross-magnetization [4] and some researchers account for the effect of cross-magnetization [19]. The effect of the saturation is neglected in [20], [21] while the authors in [22], [23] have taken the effect of saturation along the quadrature axis into account and disregarded saturation along the direct axis.

### 1.1.3 Saturation

In the analysis of the transient performance of saturated permanent magnet synchronous machines using the two-axis (d- and q-axis) frame model, particularly during the first few cycles after the occurrence of the fault (the subtransient period), the accurate calculation of the stator and rotor damper winding currents, the air-gap torque and the load angle depends on the saturation condition of their main flux paths [24], [25]. Interior permanent magnet synchronous machines have larger ferromagnetic path along the quadrature axis and, as a result, the q-axis magnetizing reactance saturates significantly under normal operating conditions [26]. On the other hand, the effect of saturation along the direct axis is usually ignored as the effective air-gap path length along the direct axis is large [1], [22], [27]. Since the relative magnetic permeability of the permanent magnet is close to unity, the magnetic reluctance along the quadrature axis is considerably smaller compared with the magnetic reluctance along the direct axis [28]. Consequently, the interior permanent magnet synchronous machines present inverse saliency and the q-axis magnetizing reactance is larger than the d-axis magnetizing reactance such as  $X_{md} < X_{mq}$ . However, since there is saturation along the direct axis up to a certain level, it is important to include direct axis saturation in addition to the quadrature axis saturation for more accurate transient behavior analysis.

In this research work, the effect of the main flux saturation both in the direct and quadrature axes on the determination of the transient performances of permanent magnet synchronous machines has been demonstrated

#### **1.1.4 Electrical Transients**

The term 'transients' has been used in the analysis of power systems for a long time. Its name immediately conjures up the notion of an event that is undesirable but momentary in nature. The primary definition uses the word rapid and talks of frequencies up to 3 MHz. Other definitions simply state that a transient is "that part of the change in a variable that disappears during transition from one steady-state operating condition to another."

Broadly speaking, transients can be classified into two categories; impulsive and oscillatory [29]. These terms reflect the waveshape of a current or voltage transient. An impulsive transient is a sudden, nonpower frequency change in the steady-state condition of voltage, current or both, that is unidirectional in polarity (primarily either positive or negative). The most common cause of impulsive transients is lightning. Fig. 2 illustrates a typical current impulsive transient caused by lightning.

An oscillatory transient consists of a voltage or current whose instantaneous value changes polarity rapidly. It is described by its spectral content (predominant frequency), duration, and magnitude as shown in Fig.3.

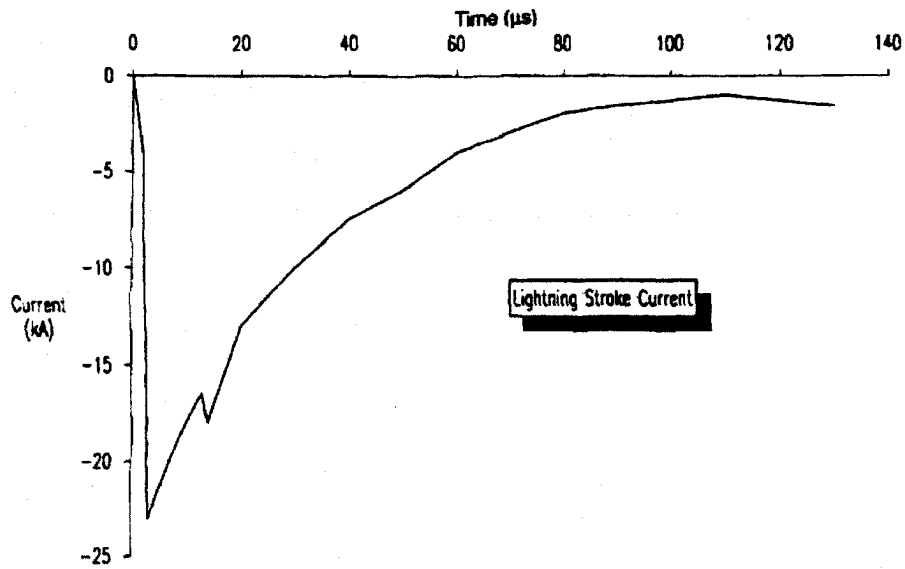


Fig. 2. Lightning stroke current that can result in impulsive transients on the power system [29].

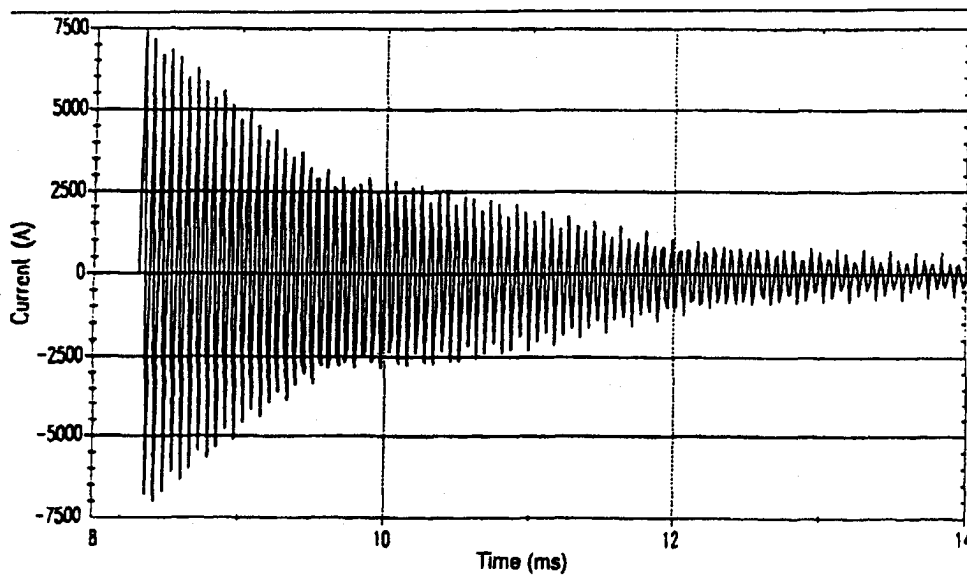


Fig. 3. Oscillatory transient caused by back-to-back capacitor switching [29].

Electrical transients can include other terms such as short duration variations. This category encompasses voltage sags or swells, and each type can be designated as instantaneous, momentary, or temporary depending on its duration as shown in Figs. 4-6.

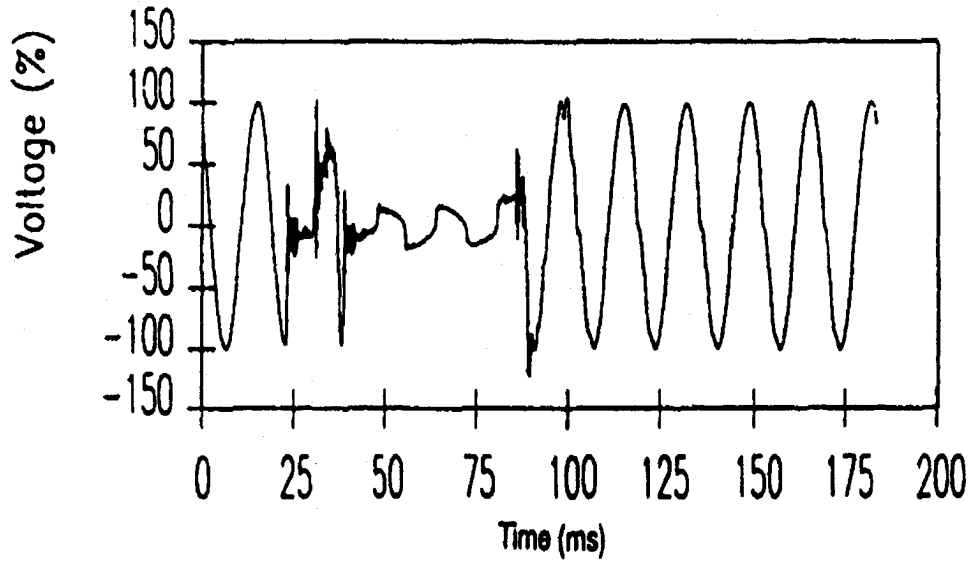


Fig. 4. Instantaneous voltage sag caused by a SLG fault [29].

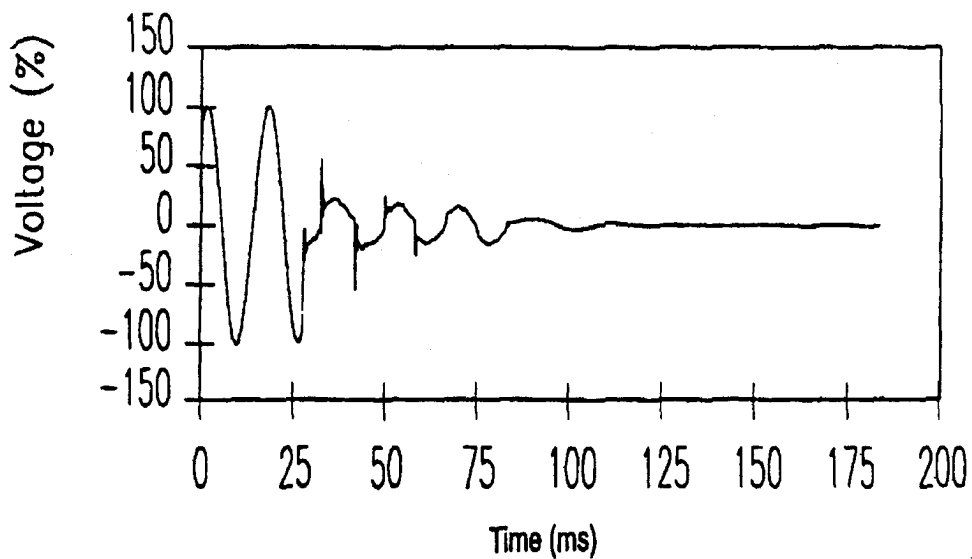


Fig. 5. Momentary interruption due to a fault and subsequent recloser operation [29].

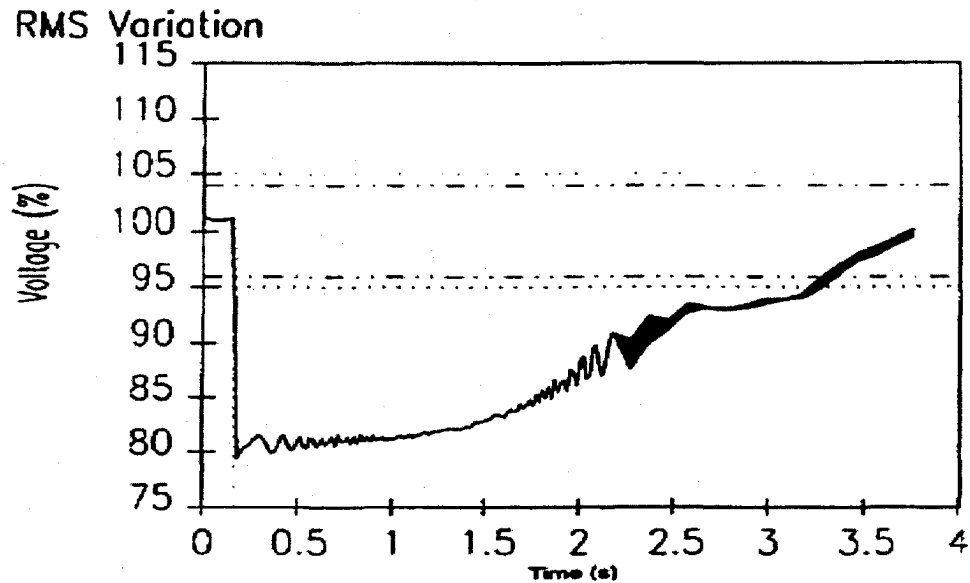


Fig.6. Temporary voltage sag caused by motor starting [29].

As mentioned above electrical transients can be classified according to the duration

as:

1) Instantaneous

- 1.1) sag for a duration of 0.5-30 cycles
- 1.2) swell for a duration of 0.5-30 cycles

2) Momentary

- 2.1) sag for a duration of 30 cycles-3 sec
- 2.2) swell for a duration of 30 cycles-3 sec

3) Temporary

- 3.1) sag for a duration of 3 sec-1 min
- 3.2) swell for a duration of 3 sec- 1 min



Modeling of permanent magnet synchronous motors has been examined and useful results have been reported in [30]-[35]. However, the effect of electrical transient and the dynamic performance have not been widely investigated on the permanent magnet synchronous machine [2]. In this research work electrical transients such as short-circuit, sag, and swell will be applied to a typical permanent magnet synchronous machine to study and analyze the effect of the electrical transients on the performance of permanent magnet synchronous machine.

Sag magnitude is the net root mean square (r.m.s) voltage available during the fault expressed in percent or in per unit of nominal voltage. Voltage sag is defined as momentary decrease in the r.m.s (rated) AC voltage (10%-90%), with a duration ranging from 0.5 cycle to 30 cycles [29]. Some common reasons for voltage sags are fault conditions within the plant or power system, short-circuits and starting of large motors that require high starting currents, large load changes, equipment failures, accidental contact with power lines, or intermittent loose connections in power wiring and it lasts until the fault is cleared [36]-[43]. Severe sags can result in the malfunctioning of some sensitive loads, cause large torque peaks in electrical machines or may cause tripping of the machine by the action of the undervoltage protection or overcurrent protection relays and the longer the voltage sag lasts, the more probable the chances of malfunction [44], [45]. Voltage sags can be characterized by their magnitude (voltage during the fault) and their duration [46]-[48]. The magnitude is determined by the electrical distance to the fault and duration by the fault clearing time. Magnitude and duration are two essential and important sag characteristics which determine the equipment behavior. Figure 7 illustrates typical instantaneous voltage sag of duration of 3 cycles (50 ms). In this figure

the voltage amplitude during the sag drops to a value of 20% (80% reduction) of the pre-sag voltage and post-sag voltage returns after the sag duration to its pre-sag value [49], [50].

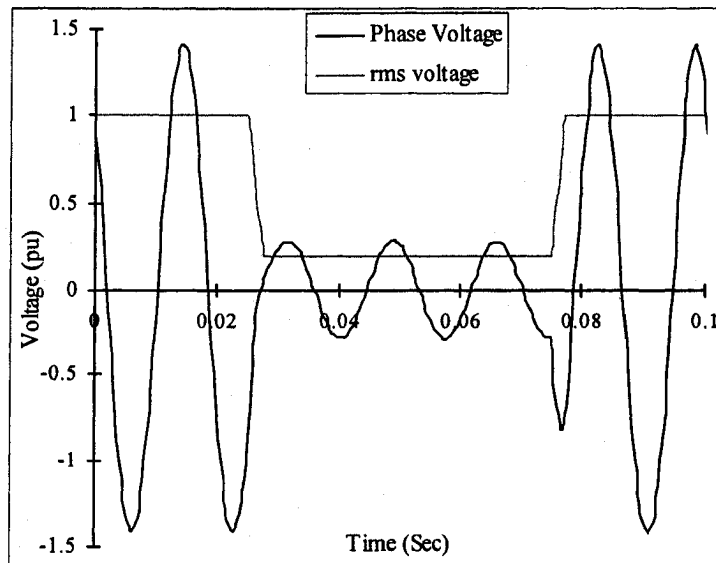


Fig. 7. Voltage sag in one phase for duration of 50 ms

When a three-phase permanent magnet synchronous machine is subjected to a sudden three-phase-to-ground short-circuit at its terminals, asymmetrical, short-circuit currents will flow in its stator and rotor damper windings. The resulting transient short-circuit currents are determined by the internal voltage of the motor and by the system impedance between the machine internal voltage and the fault. These asymmetrical transient short-circuit currents may be several orders of magnitude larger than normal operating currents and if allowed to persist may cause the motor thermal damage. These transient short-circuit currents have mainly two components: a symmetrical ac component and a dc component. While the fundamental frequency ac component decays to the sustained ac

steady-state short-circuit current, the dc component decays to zero at a relatively faster rate. The initial values of the dc components of the stator currents differ in magnitude in the three phases of the stator winding, but they decay at the same exponential rate. The unequal dc currents in the three stator phases give rise to fundamental component currents in the rotor damper windings. The values of the dc components in the three stator phases depend on the particular point in the cycle at which the short circuit occurs [36],[51].

Instantaneous voltage swells are short duration increase (110% - 180%) in the root mean square (rms) voltage magnitude and lasting from 0.5 cycle to 30 cycles, and are usually associated with systems disturbances such as switching off a large load or energizing a large capacitor bank or by faults produced within power systems [35]. Voltage swells are usually characterized by the swell magnitude and the duration of the swell [52]-[54]. If a permanent magnet synchronous machine is subjected to instantaneous voltage swell, high torque peaks may damage the machine shaft or equipment connected to the shaft. Also, it is possible that the voltage swell may cause overheating, destruction of equipment or even tripping and machine shut down by the action of the overvoltage protection or overcurrent protection relays. Voltage swells might not be as common as voltage sags, however are much more harmful to some power equipments. Figure 8 illustrates a typical instantaneous voltage swell of duration of 3 cycles (50 ms). In this figure, the voltage amplitude during the swell increases to a value of 150% of the pre-swell voltage and the post-swell voltage returns after the swell duration to its pre-swell value.

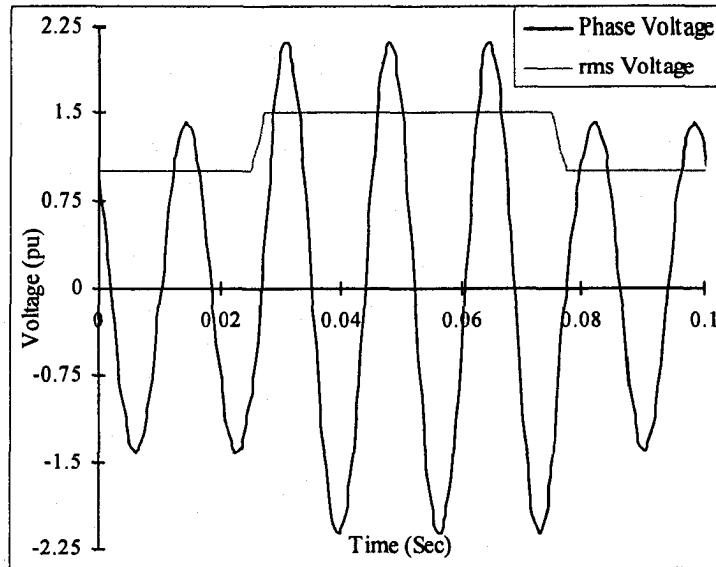


Fig. 8. Voltage swell in one phase for duration of 50 ms.

### 1.1.5 Voltage Profile

Transient voltage profile at the terminal of an electrical machine is usually represented by a rectangular shape [55]. In this case, the occurrence of the fault is represented by an immediate fall of the machine terminal voltage from its pre-fault value to the fault value (short-circuit/sag/swell) and the clearing of the fault is represented by an immediate recovery of the terminal voltage from fault (short-circuit/sag/swell) value to a post-fault value. However, in reality, when fault occurs or when it is cleared, the machine terminal voltage does not change instantly, but rather it takes a certain period of time to reach to fault or a post-fault value due to the reactive elements of the system. In their effort to prevent instantaneous changes in voltage (due to capacitors) and current (due to inductors), the network reactive elements establish voltage fall/recovery periods [56]-[58]. In the analysis of voltage profile, one of the severest fault types will be applied to the machine, namely three-phase short-circuit fault.

## **1.2 Objective**

The aim of this research work is to demonstrate the importance of the inclusion both d- and q-axis saturation on the transient behavior of permanent magnet synchronous machines in the case of a fault (i.e. bolted three-phase symmetrical short circuit, voltage sag, and voltage swell).

Moreover, this research work proposes a voltage profile due to fault at the machine terminals considering the terminal voltage fall and recovery durations. Also, the effect of the proposed transient voltage profile on the performance of saturated permanent magnet synchronous machines will be demonstrated.

In addition, the goal of the work presented in this research is to demonstrate that the impact of voltage sag/swell magnitude and duration on the transient behavior of saturated permanent magnet synchronous machines.

## **1.3 Scope**

For a specific known load torque, frequency, real and reactive power, and terminal voltage; it is required to predict the current that will flow in the stator winding as well as the electromagnetic torque for machine analysis. In this case, there is no direct solution to the equations that describe the phasor diagram and instead a solution can only be obtained by using a step by step integration method. A computer program has been developed to solve the nonlinear equations using a standard numerical integration technique with an iterative procedure based on Runge-Kutta algorithm. Therefore, a general model (with two methods) of interior permanent magnet synchronous machines

has been developed using the permanent magnet synchronous machine equations. The back electromotive force produced by a permanent magnet synchronous machine can be assumed to be equivalent to the one produced by an excitation coil. Hence the mathematical model of a permanent magnet synchronous machine is similar to that of the conventional synchronous machine [16]. As mentioned above the developed general unsaturated model, can be solved using two methods. In the first method, flux differential equations have been used and in the second method, current differential equations have been used.

Using the proposed unsaturated model; two other models representing the main flux saturation are developed. In the second model, one saturation factor is used to modify the unsaturated q-axis magnetizing reactance. This q-axis saturation factor can be determined from the q-axis saturation characteristic corresponding to the q-axis magnetizing ampere-turns. In the third model, two saturation factors are used to modify the unsaturated q- and d-axis magnetizing reactances. These q- and d-axis saturation factors can be determined from their respective q- and d-axis saturation characteristics corresponding to the q- and d-axis magnetizing ampere-turns. A comparison will be made between the results calculated by using these three models to demonstrate how important it is to include saturation in both d- and q-axis for more accurate dynamic performance prediction of the permanent magnet synchronous machine.

Electrical transients are short-circuiting, sag, and swell and generally, caused by fault in the electrical system and can cause electrical machine damage if they are allowed to persist. Since the effect of electrical transient and the dynamic performance have not been widely investigated on the permanent magnet synchronous machine, this research work is

an attempt to study and analyze the transient behavior of permanent magnet synchronous machines. When a fault (i.e. three-phase symmetrical short-circuit, voltage sag, and voltage swell) is occurred at the terminals of the machine, the system reactive elements establish fall/recovery durations during the initiation and clearing of the fault. In this thesis, the effect of the voltage fall/recovery durations on the transient performance of saturated permanent magnet synchronous machines is also investigated.

## 2. Problem Definition

### 2.1 Modeling of Permanent Magnet Synchronous Machines

The published methods of solving the two-axis equivalent circuit are based upon a known input of load angle. However, in practice, a permanent magnet synchronous machine will be operated at a fixed terminal voltage and frequency, loaded at some torque and all other quantities are generally unknown including the load angle. These difficulties can be overcome by using analysis techniques that avoid the use of load angle. This research work shows that it is possible to accurately model the two-axis equivalent circuit without using the load angle technique. Through the use of iterative procedure, a solution to the two-axis model of a permanent magnet synchronous machine is obtained which does not require an input of load angle but allows for the parameter variations. The solution is able to predict machine current, speed, load angle and air-gap torque. The assumption that q-axis synchronous reactance  $X_q$ , or d-axis synchronous reactance  $X_d$ , are constant and are unaffected by saturation can lead to significant errors in the machine performance predictions [4].

As discussed before, different permanent magnet synchronous machine models have been developed by many researchers. Some being complex, not precise, especially that the synchronous nature of these machine, has led to problems in obtaining good dynamic performance [59]. But in this research work, an original approach to modeling and analysis of permanent magnet synchronous machine is presented, with special attention to the determination of its dynamic and transient behavior. So, to carry out the investigations, a computer model (using two methods) for an unsaturated permanent



magnet synchronous machine has been developed such as:

- 1) Method 1: Using the machine flux linkage differential equations to calculate transient air-gap torque, speed, load angle, stator and rotor currents, etc.
- 2) Method 2: Using the machine current differential equations to calculate transient air-gap torque, speed, load angle, stator and rotor currents, etc.

## 2.2 Saturation

In interior permanent magnet synchronous machines, since the effective air-gap length on the quadrature axis is small, the saturation in this axis is significant. On the other hand, the relative magnetic permeability of the permanent magnet is close to unity so, the effective air-gap length on the direct axis is large and the variation of the corresponding magnetizing reactance  $X_{md}$ , due to magnetic saturation, is minimal, but there is saturation up to certain extent [60] in this axis. In the two-axis (d- and q-axis) frame transient analysis of these machines, usually the impact of the saturation, especially the effect of the d-axis saturation is ignored. As rather large values of current flow in the stator circuits of a permanent magnet synchronous machine, a sort of flux redistribution occurs due to saturation and this happens even at no-load operations. Modification of the reluctance of the main flux path especially on the quadrature axis is the most important effect of saturation and it can be taken into account by changing  $X_{mq}$  according to the saturation curve in the quadrature axis [61], [62]. This research work demonstrates the effect of the main flux saturation both in the direct and quadrature axes on the determination of the transient performances of permanent magnet synchronous machines.

Furthermore, this thesis presents a model that ignores saturation (using two methods) in the machine and two more models that consider the effect of the main flux saturation.

So, three models will be investigated such that:

Model 1: saturation is ignored

Model 2: saturation only in the quadrature axis is considered

Model 3: saturation in both the direct and quadrature axes is considered

A comparison will be made between the results calculated by the three models to show the importance of inclusion of saturation in both direct and quadrature axes for more accurate dynamic performance prediction of the permanent magnet synchronous machine.

### **2.3 Electrical Transients**

Electrical transient as described in [29] is an event that is undesirable but could be classified as being instantaneous, momentary, or temporarily in nature. Electrical transient though is a problem for electrical power systems and could lead to misoperation of electrical equipment in the power system, overheating, damaging of electrical machine, tripping of the machine or possible shut down. Even though, understanding and being able to predict the dynamic performance of permanent magnet synchronous machine subjected to an electrical transient is essential; the effect of electrical transients on the machine dynamic performance has not been widely investigated.

So, in this research work three types of electrical transients (such as, short-circuit, voltage sag, and voltage swell) will be investigated in order to have better understanding and analysis of the transient behavior of permanent magnet synchronous machines.

## 2.4 Voltage Profile

As mentioned in the introduction, during the occurrence and clearing of fault, the machine terminal voltage does not change instantly but rather it takes some time to reach fault or a post-fault value. The reactive elements of the system, in their effort to prevent instantaneous change in voltage due to the presence of capacitors and instantaneous change in current due to the presence of inductors, establish voltage fall and recovery durations of the pulse waveform as shown in Figs. 9(a-c). The most commonly used transient voltage profile is illustrated in Fig. 9(d) [55]. The voltage fall and recovery durations in Figs. 9(a-c) have been represented by exponential function in [56] and by immediate fall/recovery then exponential function in [57], [58] as shown in Figs. 9(b) and 9(c), respectively. In [57], a voltage fall/recovery duration of 90 ms was used, while in [58], a voltage fall/recovery duration of 200 ms was used. The effect of the voltage fall and recovery durations on the machine performance was not demonstrated in these papers. This thesis proposes a transient voltage profile which will be used to investigate the effect of the voltage fall and recovery durations on the machine transient performance.

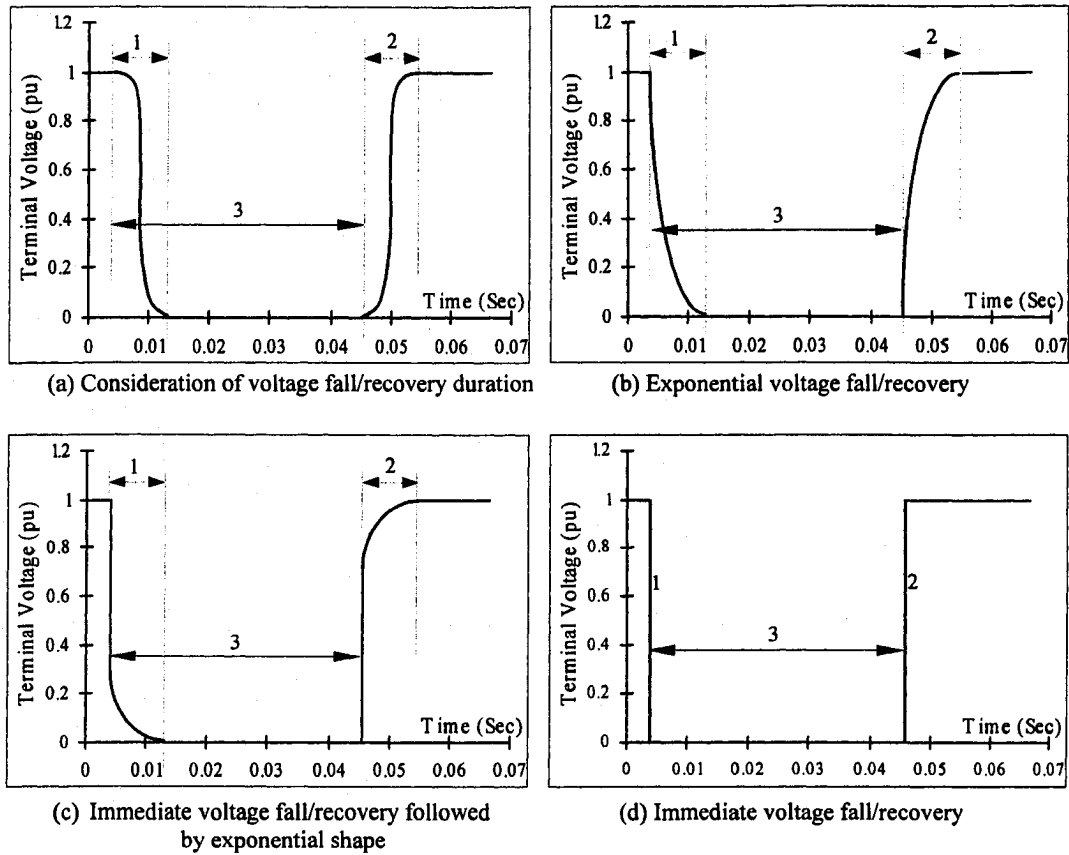


Fig. 9. Numerous voltage profiles to represent the occurrence and clearing of a short-circuit fault.

- |   |
|---|
| <ol style="list-style-type: none"> <li>1. Voltage fall duration from steady-state value to fault value</li> <li>2. Voltage recovery duration from fault value to a post-fault value</li> <li>3. Fault duration</li> </ol> |
|---|

### 3. PMSM Modeling for Electrical Transient Analysis

#### 3.1 Equivalent Circuits

The d- and q-axis equivalent circuits of permanent magnet synchronous machine are shown in Fig. 10. The machine phasor diagram is illustrated in Fig. 11. One damper winding in the direct axis and one damper winding in the quadrature axis have been considered.

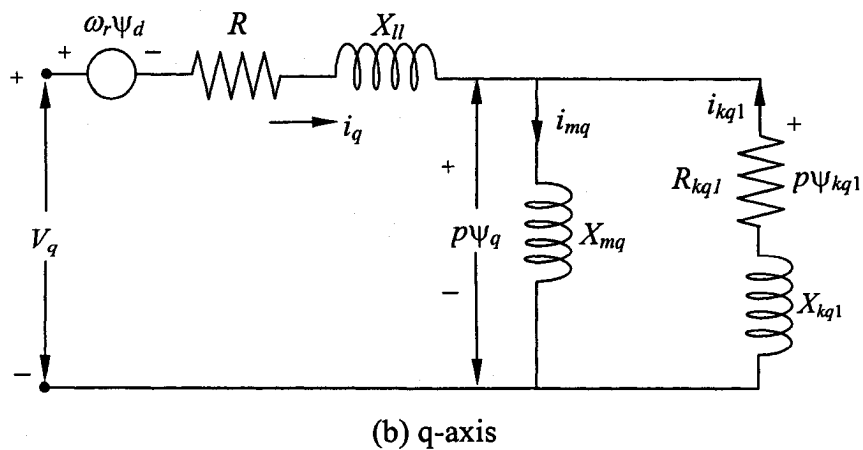
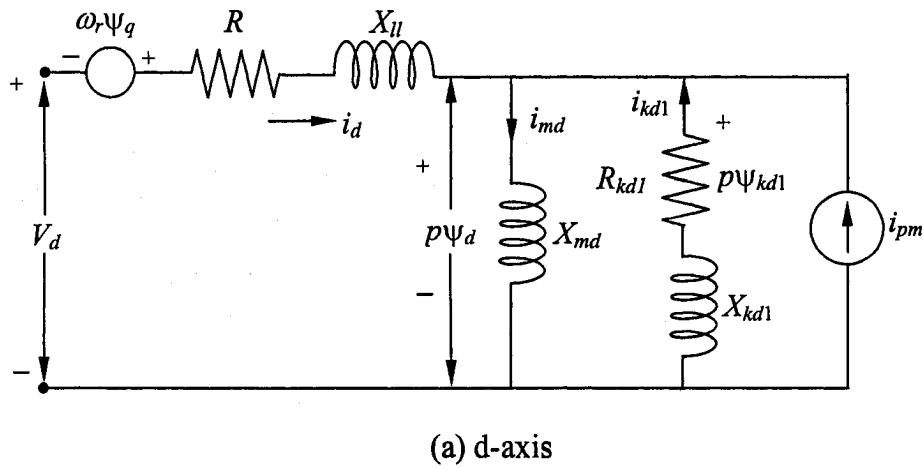
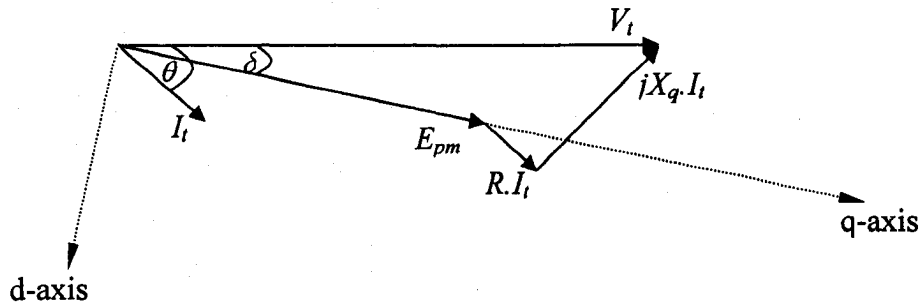
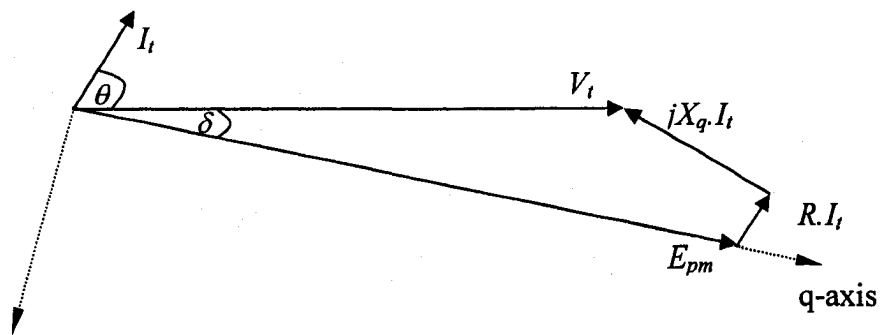


Fig. 10. d- and q-axis equivalent circuits.



a) Lagging power factor



b) Leading power factor

Fig. 11. Machine phasor diagram

The following assumptions in the development of the models are made:

- (a) Effect of iron, stray losses and mutual coupling effects between d- and q-axis are assumed negligible.
- (b) The machine permanent magnet excitation has been represented by an equivalent current source as that presented in reference.
- (c) The machine operated from a balanced source.
- (d) The machine speed is variation is considered.

### 3.2 Unsaturated Model

A model for unsaturated permanent magnet synchronous machines has been developed for the following two cases:

- 1) Using the flux differential equations and
- 2) Using the current differential equations.

#### 3.2.1 Model Using Flux Differential Equations

The permanent magnet synchronous machine stator and rotor circuit voltage equations can be expressed in the following form:

$$\left. \begin{aligned} \frac{d\psi_d}{dt} &= V_d + R i_d + \omega_r \psi_q \\ \frac{d\psi_q}{dt} &= V_q + R i_q - \omega_r \psi_d \\ 0 &= R_{kd1} i_{kd1} + \frac{d\psi_{kd1}}{dt} \\ 0 &= R_{kq1} i_{kq1} + \frac{d\psi_{kq1}}{dt} \end{aligned} \right\} \quad (1)$$

The mechanical equations can be expressed as

$$\left. \begin{aligned} \frac{d\omega_r}{dt} &= \frac{(T_m - T_e)}{J} \\ \frac{d\delta}{dt} &= \omega_s (\omega_r - 1) \end{aligned} \right\} \quad (2)$$

where

$$T_e = \psi_d i_q - \psi_q i_d \quad (3)$$

In the determination of the transient performance due to fault at the machine terminals, the initial steady-state values of the machine currents and flux linkages are calculated first for a particular loading condition. To simulate the effect of the fault, the

d- and q-axis components of the terminal voltage  $V_d$  and  $V_q$  in (1) are made equal to fault values. These initial steady-state values of the currents, flux linkages, speed and load angle at the beginning of the time step are used to find the flux linkages, speed and load angle.

The calculated flux linkages at the beginning of the step are then used to calculate the armature (stator) and damper winding (rotor) currents at the end of the step by using following the permanent magnet synchronous machine current equations:

$$\begin{bmatrix} i_d \\ i_q \\ i_{kd1} \\ i_{kq1} \end{bmatrix} = \begin{bmatrix} -(X_{mdu} + X_{ll}) & 0 & X_{mdu} & 0 \\ 0 & -(X_{mqu} + X_{ll}) & 0 & X_{mqu} \\ -X_{mdu} & 0 & (X_{mdu} + X_{kd1}) & 0 \\ 0 & -X_{mqu} & 0 & (X_{mqu} + X_{kq1}) \end{bmatrix}^{-1} \begin{bmatrix} \psi_d \\ \psi_q \\ \psi_{kd1} \\ \psi_{kq1} \end{bmatrix} - \begin{bmatrix} \psi_{pm} \\ 0 \\ \psi_{pm} \\ 0 \end{bmatrix} \quad (4)$$

### 3.2.2 Model Using Current Differential Equations

The permanent magnet synchronous machine stator and rotor circuit current differential equations can be expressed in the following form:

$$\begin{bmatrix} \frac{di_d}{dt} \\ \frac{di_q}{dt} \\ \frac{di_{kd1}}{dt} \\ \frac{di_{kq1}}{dt} \end{bmatrix} = \omega_s \begin{bmatrix} -(X_{mdu} + X_{ll}) & 0 & X_{mdu} & 0 \\ 0 & -(X_{mqu} + X_{ll}) & 0 & X_{mqu} \\ -X_{mdu} & 0 & (X_{mdu} + X_{kd1}) & 0 \\ 0 & -X_{mqu} & 0 & (X_{mqu} + X_{kq1}) \end{bmatrix}^{-1} \begin{bmatrix} V_d + R \cdot i_d - \omega_r (X_{mqu} + X_{ll}) i_q + \omega_r X_{mqu} i_{kd1} \\ V_q + R \cdot i_q + \omega_r (X_{mdu} + X_{ll}) i_d - \omega_r X_{mdu} i_{kd1} - \omega_r X_{mdu} i_{pm} \\ -R_{kd1} i_{kd1} \\ -R_{kq1} i_{kq1} \end{bmatrix} \quad (5)$$



The mechanical equations and electromagnetic equations are given in (2) and (3), respectively.

In the determination of the transient performance due to fault at the machine terminals, the initial steady-state values of the machine currents and flux linkages are calculated first for a particular loading condition. To simulate the effect of the fault, the d- and q-axis components of the terminal voltage  $V_d$  and  $V_q$  in (1) are made equal to fault values.

The differential equations in (2) and (5) are solved using the 4<sup>th</sup>-order Runge-Kutta method. These calculated current differential equations at the beginning of the step are then used to calculate the armature (stator) and damper winding (rotor) flux at the end of the step by using following the permanent magnet synchronous machine flux equations:

$$\begin{bmatrix} \psi_d \\ \psi_q \\ \psi_{kd1} \\ \psi_{kq1} \end{bmatrix} = \begin{bmatrix} -(X_{mdu} + X_{ll}) & 0 & X_{mdu} & 0 \\ 0 & -(X_{mqu} + X_{ll}) & 0 & X_{mqu} \\ -X_{mdu} & 0 & (X_{mdu} + X_{kd1}) & 0 \\ 0 & -X_{mqu} & 0 & (X_{mqu} + X_{kq1}) \end{bmatrix} \begin{bmatrix} i_d \\ i_q \\ i_{kd1} \\ i_{kq1} \end{bmatrix} + \begin{bmatrix} X_{mdu} i_{pm} \\ 0 \\ X_{mdu} i_{pm} \\ 0 \end{bmatrix} \quad (6)$$

The calculated currents, flux linkages, speed and load angle at the end of the step can be used to find the transient performance for the next time step. Upon restoration of the normal voltage,  $V_d$  and  $V_q$  in (1) are calculated using the new post-fault voltage and the machine load angle. The calculation of the motor dynamic performance continues for the post-fault condition.

### 3.3 Saturated Machine Models

Models of permanent magnet synchronous machines considering the saturation along the direct and quadrature axes have been obtained by modifying the unsaturated model that was described in the previous section.

#### 3.3.1 Model Considering only q-Axis Saturation

In this approach, the unsaturated q-axis magnetizing reactance ( $X_{mqu}$ ) is replaced by its corresponding saturated value. This q-axis saturated magnetizing reactance  $X_{mqs}$  is obtained by modifying the corresponding unsaturated value,  $X_{mqu}$ , with saturation factor  $K_q$ , corresponding to the saturation condition along the quadrature axis as in (7). The q-axis magnetizing ampere-turns is used to locate the operating points on the q-axis saturation characteristics,

$$X_{mqs} = K_q X_{mqu}. \quad (7)$$

#### 3.3.2 Saturated Model Considering both d- and q-axis Saturation

In this case, both d- and q-axis saturation are considered. The unsaturated d- and q-axis magnetizing reactances are replaced by their corresponding saturated values. These d- and q-axis saturated magnetizing reactances,  $X_{mds}$  and  $X_{mqs}$ , are obtained by modifying the corresponding unsaturated values,  $X_{mdu}$  and  $X_{mqu}$ , with two saturation factors,  $K_d$  and  $K_q$ , corresponding to the saturation conditions along the direct and quadrature axes, respectively as in (8). The d- and q-axis magnetizing ampere-turns are used to locate the operating points on the d- and q-axis saturation characteristics, respectively.

$$X_{m ds} = K_d X_{m du} ; X_{m qs} = K_q X_{m qu} . \quad (8)$$

By applying the procedure described above, the transient performance of permanent magnet synchronous machines considering the saturation along the direct and quadrature axes can be calculated. However, in this case, an iterative technique has to be applied to determine the transient performance as the saturated d- and q-axis magnetizing reactances in (4) and (6) depend on the saturation level.

## 4. Numerical Investigation

### 4.1 System Studied and Machine Parameters

The three-phase permanent magnet synchronous machine under investigation is connected to the infinite bus through a transmission line as shown in the one line diagram in Fig. 12. A fault (i.e. three-phase short-circuit, voltage sag, or voltage swell) at the terminal of the machine occurs at 4.167 ms (or 12.5 ms) and remains for 33.33 ms.

#### 4.1.1 Machine Parameters

To investigate the effect of the faults applied (short-circuit, voltage sag, or voltage swell) on the transient performance of saturated permanent magnet synchronous machines, the proposed models have been applied to a three-phase, 4-pole, 37.5 V, 7 A permanent magnet synchronous machine [14]. The transient performance have been calculated considering and ignoring the saturation for a loading condition corresponding to active power 0.75 pu and

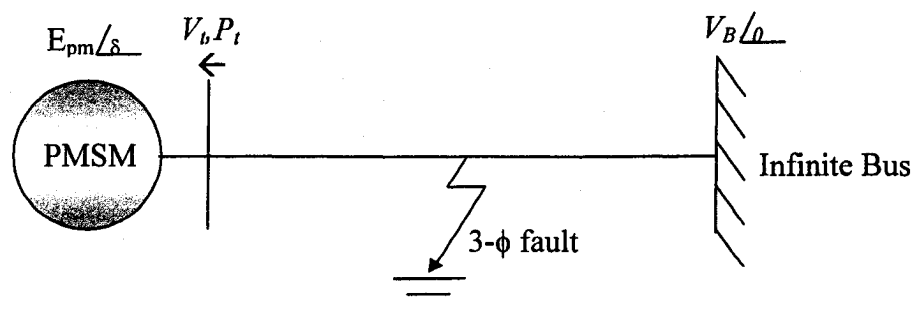


Fig. 12. Single line diagram for the system studied.

reactive power 0.5 pu under both lagging and leading power factor conditions at the terminal of the machine. The time step used in the numerical investigations is 1/2400 sec.

Table 1. Machine parameters

Rated power	0.46 kVA
Rated voltage	37.5 V
Rated current	7.0 A
Unsaturated d-axis reactance	0.366 PU
Unsaturated q-axis reactance	0.83 PU
Magnetizing d-axis reactance	0.26 PU
Magnetizing q-axis reactance	0.724 PU
Leakage reactance	0.106 PU
d-axis damper reactance	0.06 PU
q-axis damper reactance	0.06 PU
Armature (stator) resistance	0.04 PU
d-axis damper resistance	0.148 PU
q-axis damper resistance	0.148 PU

Table 2: Operating Conditions

Terminal voltage	1.0 PU
Terminal real power	0.75 PU
Terminal reactive power	0.5 PU

### 4.1.2 Machine Saturation Characteristics

The d- and q-axis saturation characteristics of the permanent magnet synchronous machine used in the investigations are shown in Fig. 13.

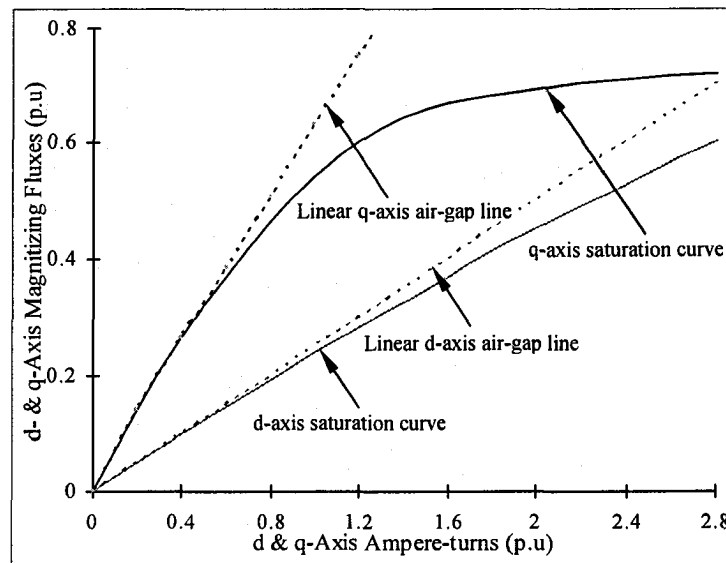


Fig. 13. d- and q-axis linear and open circuit characteristic curves.

## 4.2 Simulation Flowcharts

### 4.2.1 Procedures of Simulation

In this section, the basic procedures used to perform the initial value calculation and transient simulations by the proposed models are explained.

Figure 14 shows flowchart to calculate the initial values, where, terminal voltage, real and reactive power are given as an input. Then, the load angle ( $\delta$ ) of the machine can be calculated. Then, the d- and q axes components of the stator voltage and current, fluxes and electromagnetic torque of the machine are determined. Both method 1 and 2 in model 1 will have the same flowchart for initial value calculation.

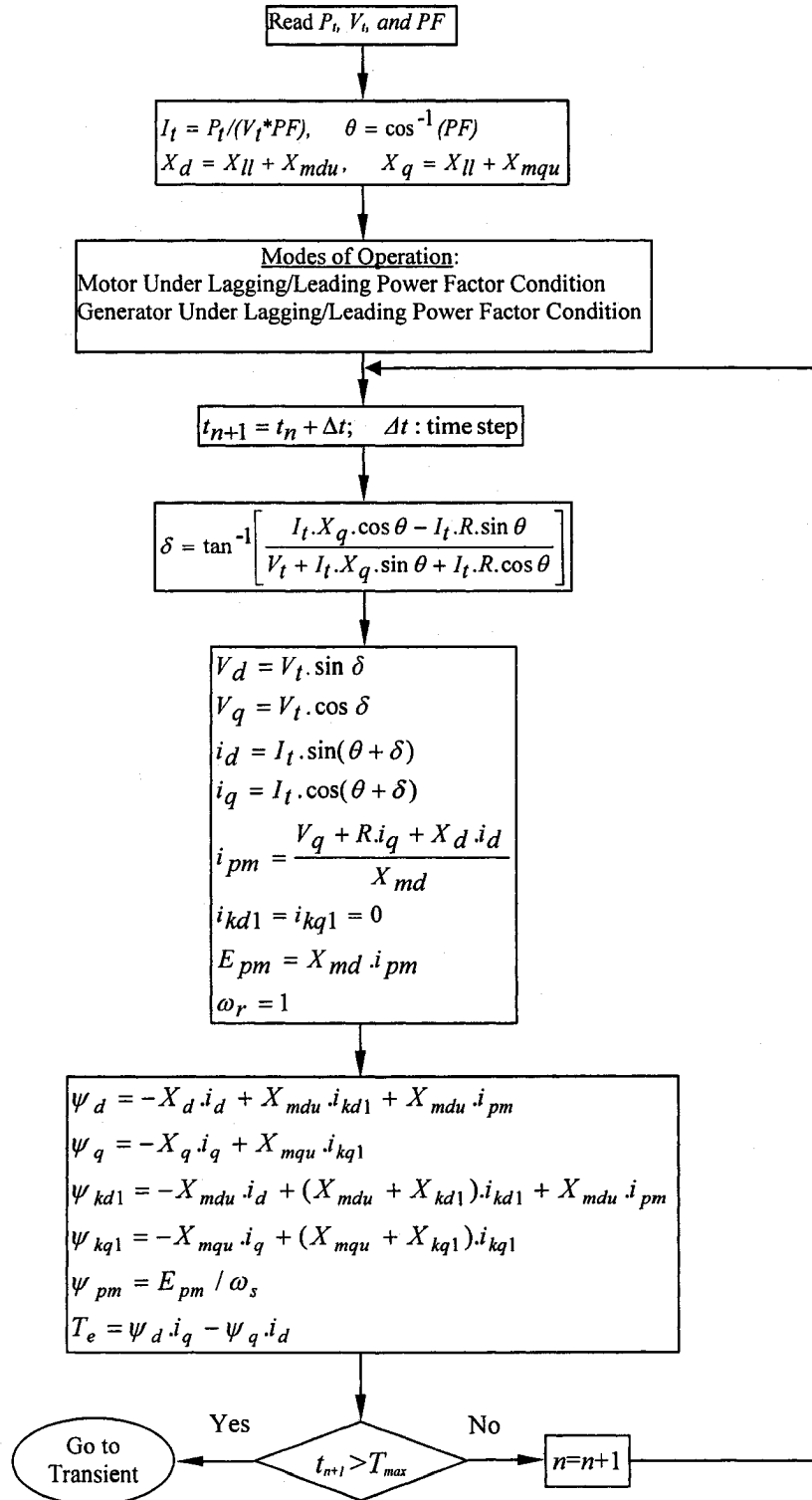


Fig. 14. Initial value calculation for the unsaturated model (methods 1 and 2 in model 1).

In general, there are two methods for the integration of differential equations in power system simulation; one is an explicit method, such as the 4<sup>th</sup> order Runge-Kutta method, and the other is an implicit one, such as the trapezoidal rule. The flowcharts shown in Figs. 15, 16, and 18 are for the explicit method. Figures 15 and 16 show flowcharts of step-by-step simulation for the calculation of transient values, such that in each of these flowcharts, fault is initiated and then sustained for a few cycles before the fault is cleared. For the method that uses flux differential equations as shown in Fig. 15, after applying Runge-Kuatta algorithm, the new values of fluxes are calculated, then, using the calculated flux values and the unsaturated reactances, current values are determined. In the case of the method using the current differential equations as shown in Fig. 16 the new values of currents are calculated, then, using the calculated current values and the unsaturated reactances, flux values are determined. The calculation of the motor dynamic performance continues for the post-fault condition.

Figure 17 illustrates the flowchart for the saturated case. The same procedures will be followed as for Fig. 14 to calculate the initial values of the d and q axes components of the stator voltage and current, fluxes and electromagnetic torque of the machine. However, in Fig. 17 for the saturated model, determination of the initial values of currents and fluxes involves an iterative process because  $X_d$  and  $X_q$  depend on the saturation level. So, after the currents converge, initial values of currents, load angle, flux linkages, etc. are determined.



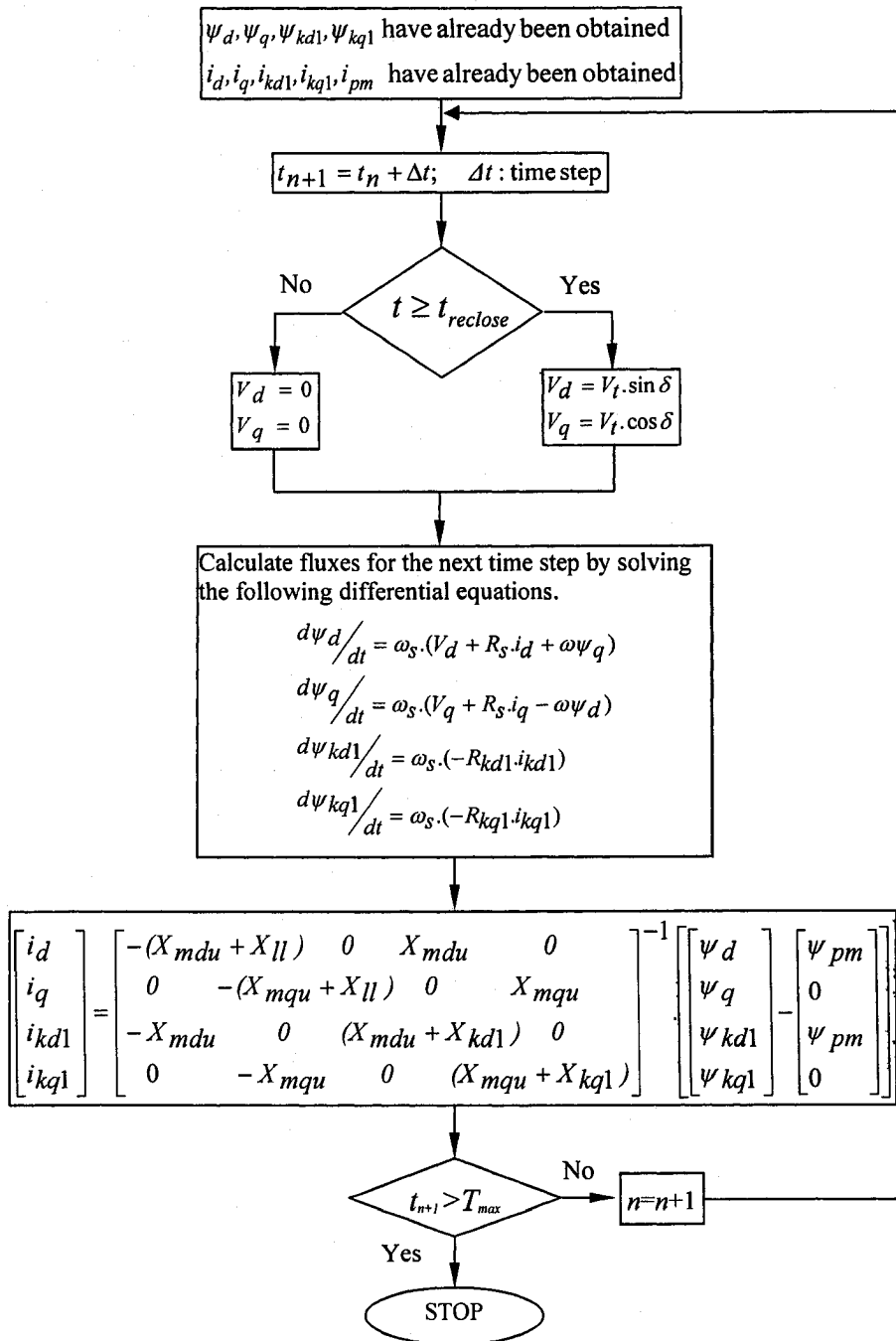


Fig. 15. Calculation of transient values using flux differential equations (method 1).

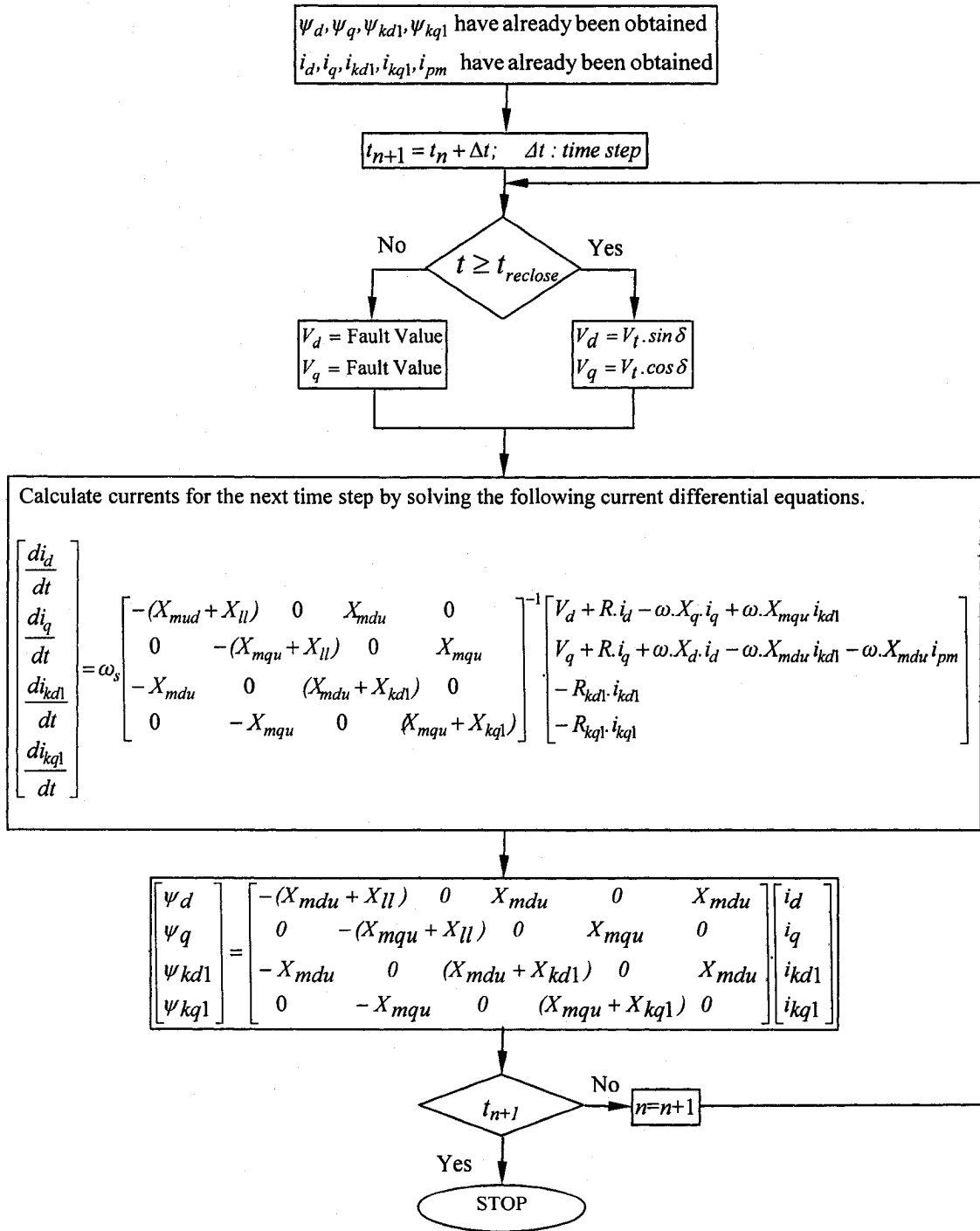


Fig. 16. Calculation of transient values using current differential equations (method 2).

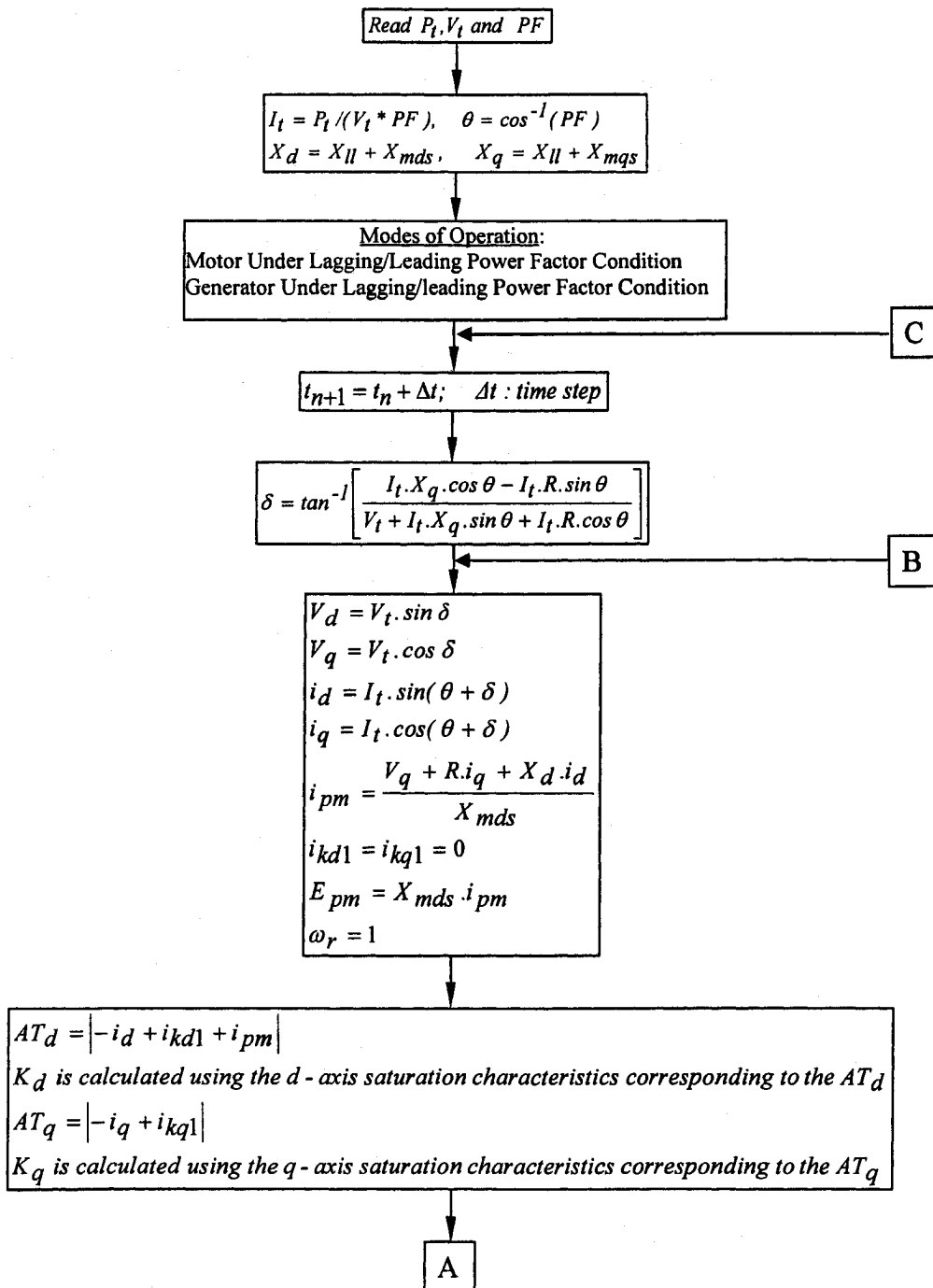


Fig. 17. Initial values calculation for models considering saturation (cont'd).

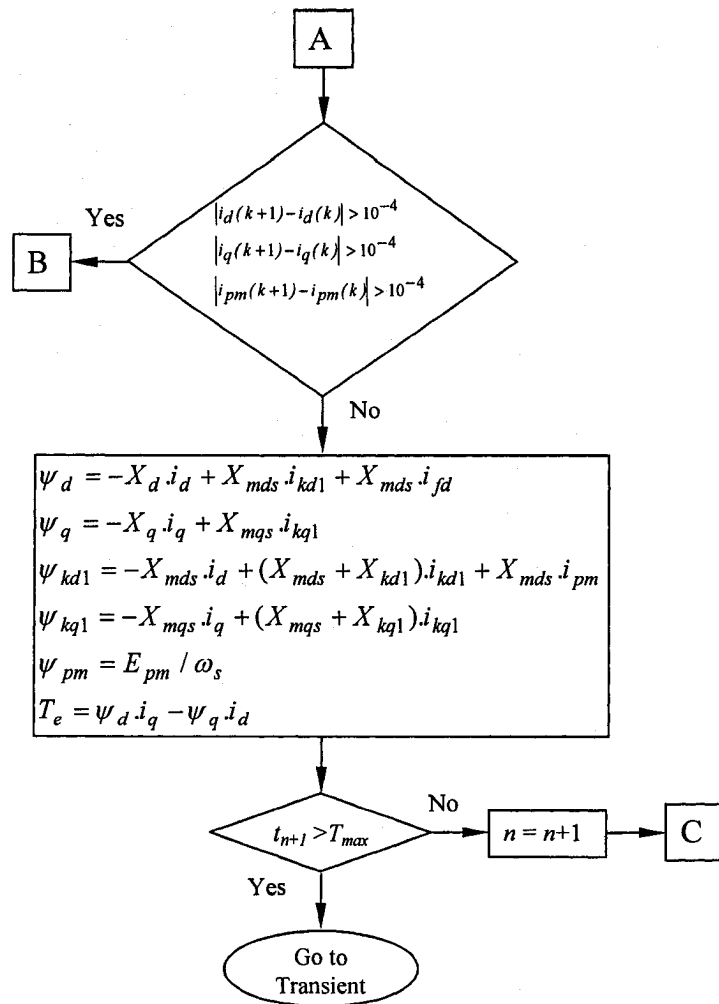


Fig. 17. Initial values calculation for models considering saturation.

Figure 18 shows flowchart of step-by-step simulation. Fault is initiated and sustained for a few cycles before it is cleared and machine terminal voltage goes back to normal value. For the method that uses flux differential equations as shown in Fig. 18, after applying Runge-Kutta algorithm, the new values of fluxes are calculated, then, currents values are determined. However, the mathematical model will be modified to take the d- and q-axis saturation (the changing of  $X_d$  and  $X_q$ ) into consideration in the iteration process in order to

calculate new magnetizing reactances and currents in each time step. Then at the end of iteration process the fluxes and currents values are determined and the program is ready to go to the next time step. The calculation of the motor dynamic performance continues for the post-fault condition.

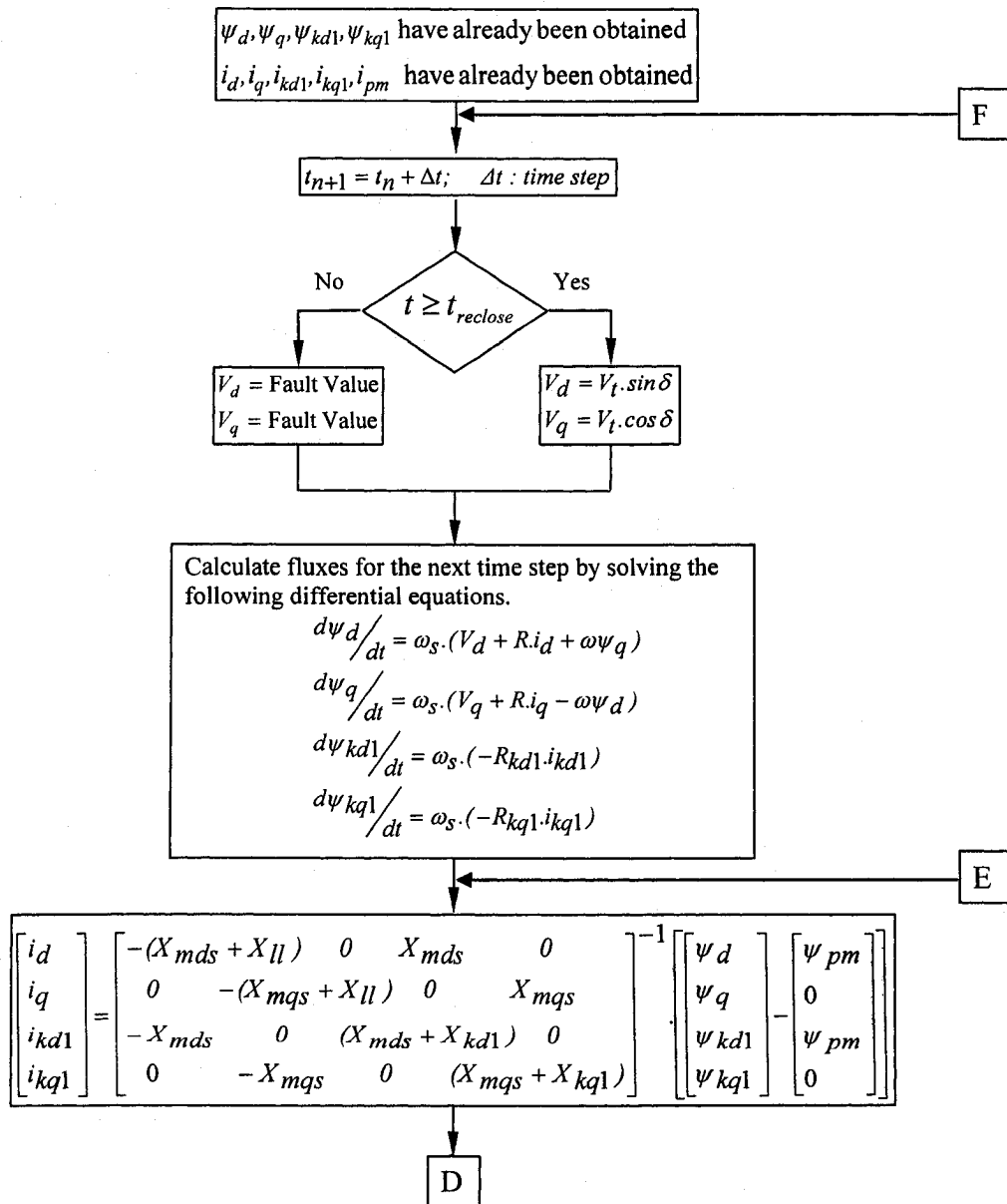


Fig. 18. Transient value calculation using flux differential equations using saturated model (cont'd).

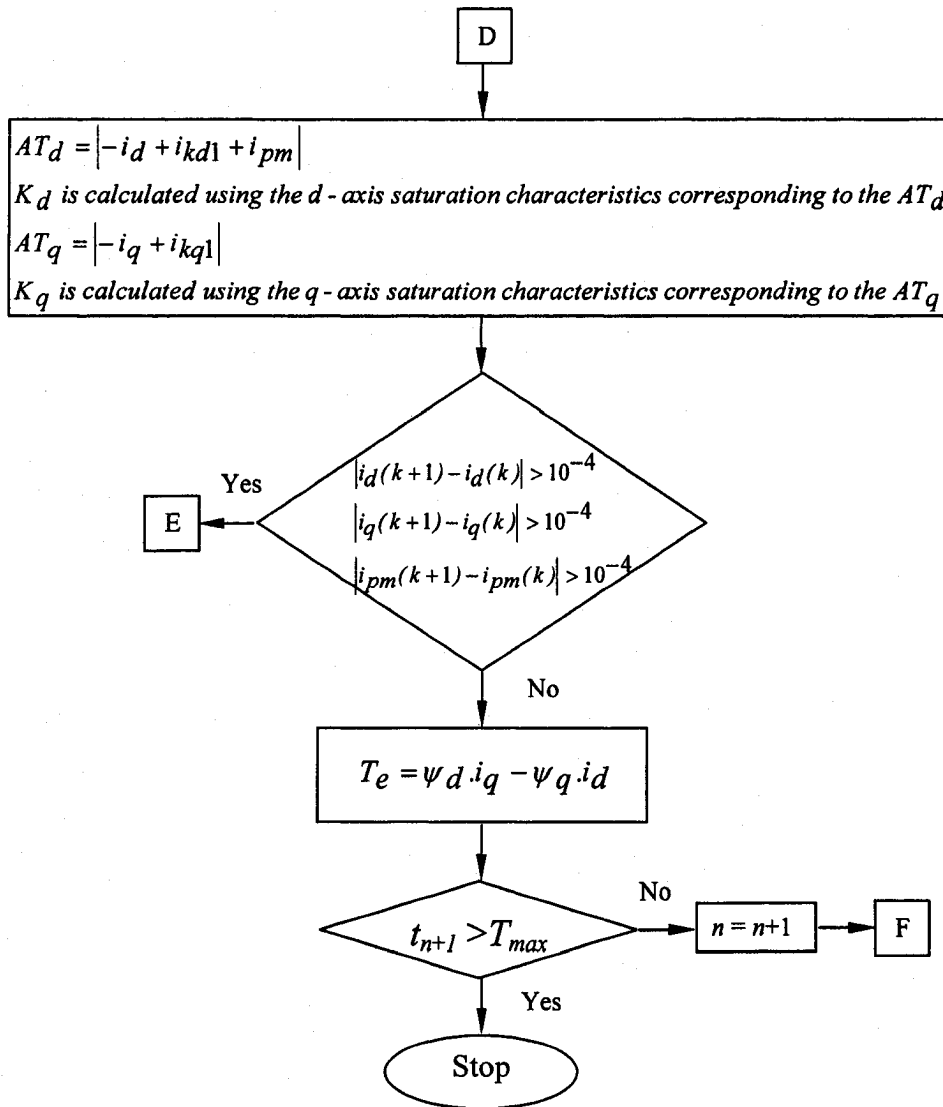


Fig. 18. Transient value calculation using flux differential equations using saturated model.

## 4.3 Numerical Calculation

### 4.3.1 Comparison of the Results Calculated by Methods 1 and 2.

To investigate the performance of the machine using model 1 (unsaturated); the proposed two methods in model 1 have been applied to a typical permanent magnet synchronous machine. In these investigations, the following are assumed:

1. A symmetrical three-phase short-circuit (SC) has been considered.
2. Upon voltage restoration, the post-SC terminal voltage comes back to the pre-short circuit voltage level 1.0 pu immediately.
3. The rotor speed remains constant and is equal to 1.0 pu.

The transient performance has been calculated ignoring the saturation for a loading condition (both generating and motoring modes of operation) corresponding to active power  $P = 0.75$  pu and reactive power  $Q = 0.5$  pu under different power factor conditions at the terminal of the machine. The pre-SC terminal voltage  $V_t$  is 1.0 pu and during the short-circuit the terminal voltage amplitude drops to 0 pu and the short-circuit continues for 41.67 ms (100 time steps). After the resumption of normal operation, the post-SC terminal voltage comes back to 1.0 pu. Figures 19 to 30 show some of the results of these investigations.

The produced air-gap torque values for the short circuit duration of 41.67ms for different machine operating conditions are shown in Figs. 19 to 22. As it can be seen from these figures, the two modeling methods produce the same air-gap torque. The post-SC peak air-gap torque has a higher negative average value for motor under leading power factor condition as shown in Fig. 20, while it has a higher positive average torque value for the same short circuit duration for generator under lagging power factor condition as shown in

Fig. 21. Also it is noticeable that when the machine is operating as a motor, the steady-state torque has negative values, since power is being absorbed from the grid. While when machine is operating as a generator, the steady-state torque has positive values, since power is being delivered to the grid.

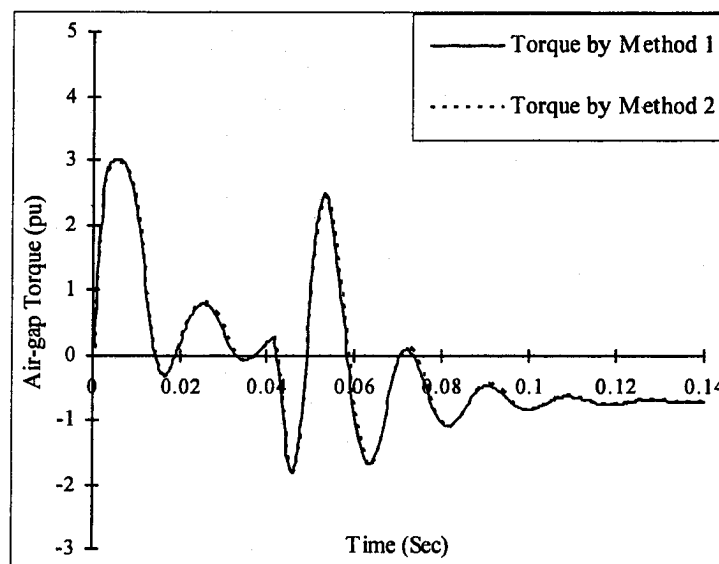


Fig. 19. Electromagnetic torque for motor under lagging power factor condition and short-circuit duration of 41.67ms.



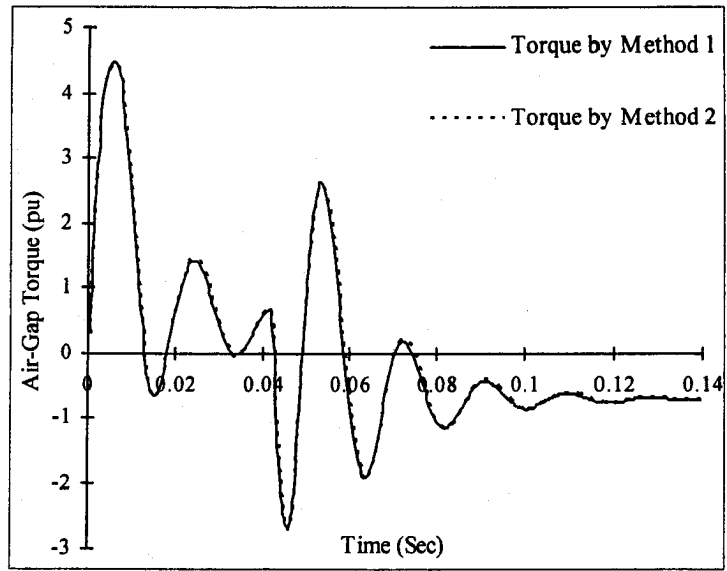


Fig. 20. Electromagnetic torque for motor under leading power factor condition and short-circuit duration of 41.67 ms.

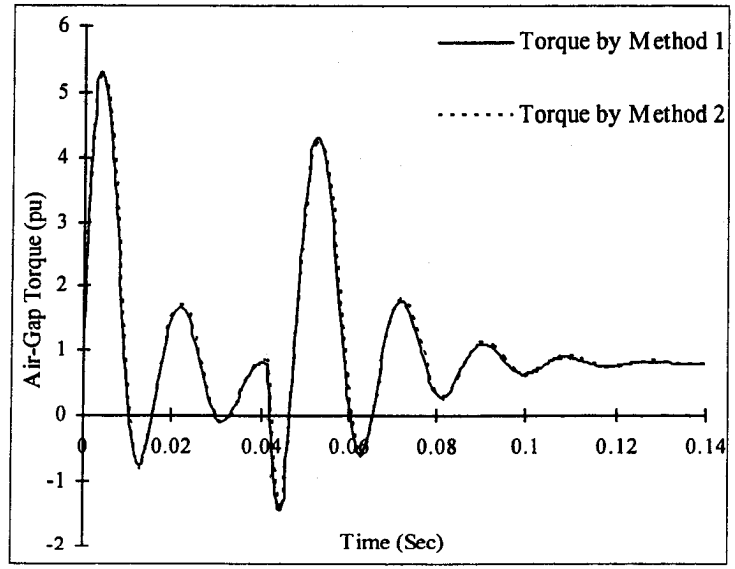


Fig. 21. Electromagnetic torque for generator under lagging power factor condition and short-circuit duration of 41.67ms.

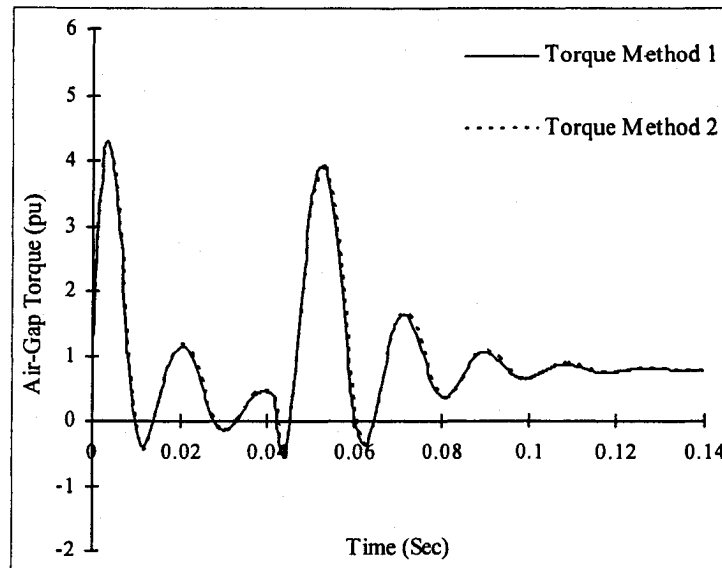


Fig. 22. Electromagnetic torque for generator under leading power factor condition and short-circuit duration of 41.67 ms.

It can be noticed from Figs. 19 to 30 for permanent magnet synchronous machine operating as motor or generator under both lagging and leading power factor conditions that method using flux differential equations yields the same results as the method using current differential equations. In order to save time and effort, only the method using flux differential equations will be used in the rest of the analysis.

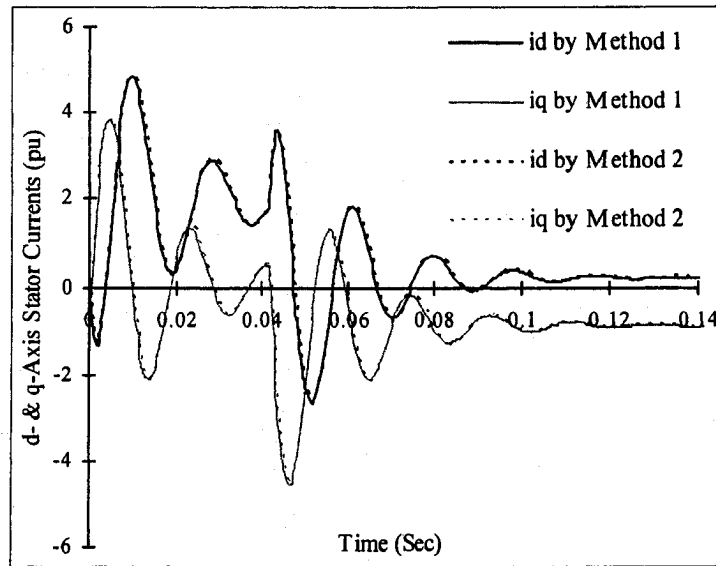


Fig. 23. d- and q-axis stator currents for motor under lagging power factor condition and short-circuit duration of 41.67 ms.

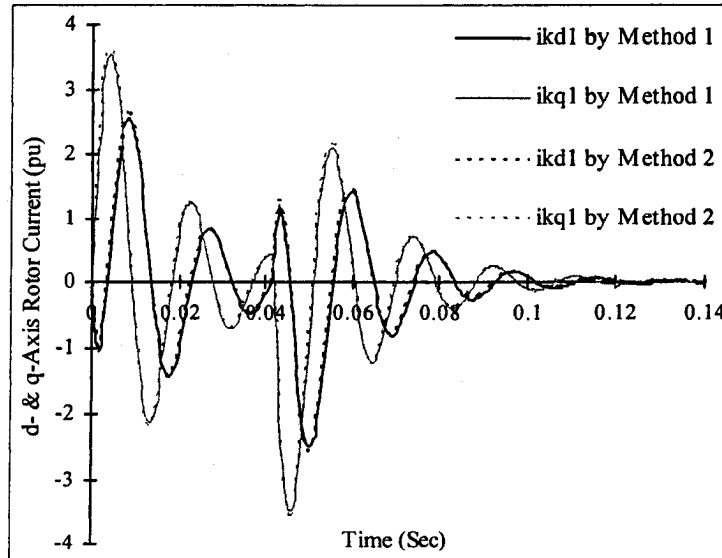


Fig. 24. d- and q-axis damper winding currents for motor under lagging power factor condition and short-circuit duration of 41.67 ms.

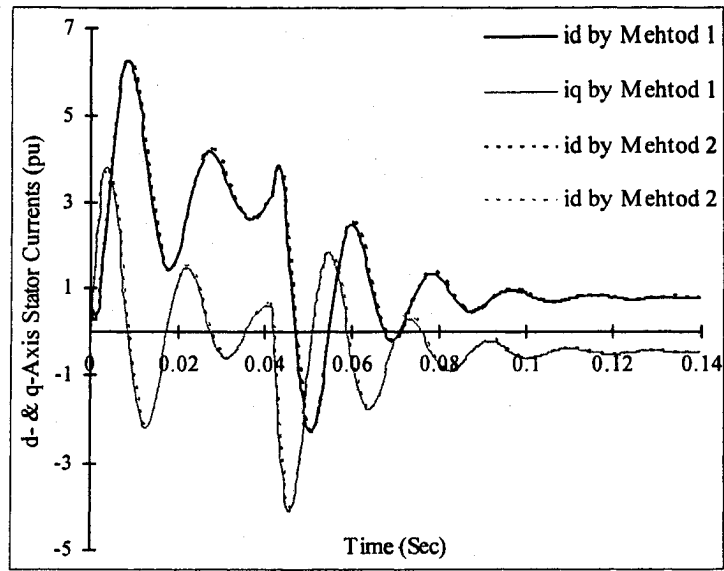


Fig. 25. d- and q-axis stator currents for motor under leading power factor condition and short-circuit duration of 41.67 ms.

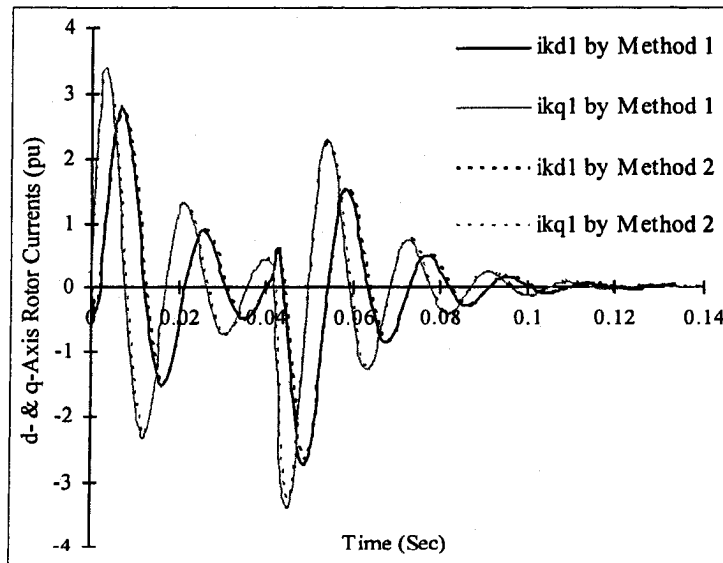


Fig. 26. d- and q-axis damper winding currents for motor under leading power factor condition and short-circuit duration of 41.67 ms.

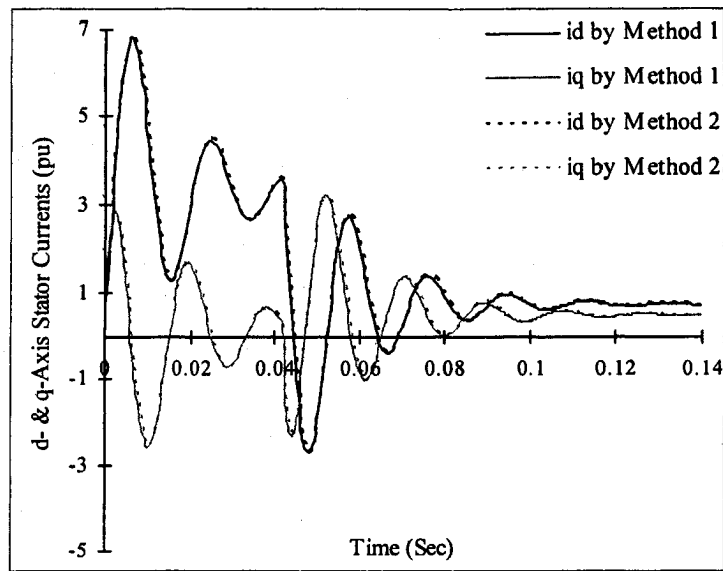


Fig. 27. d- and q-axis stator currents for generator under lagging power factor condition and short-circuit duration of 41.67 ms.

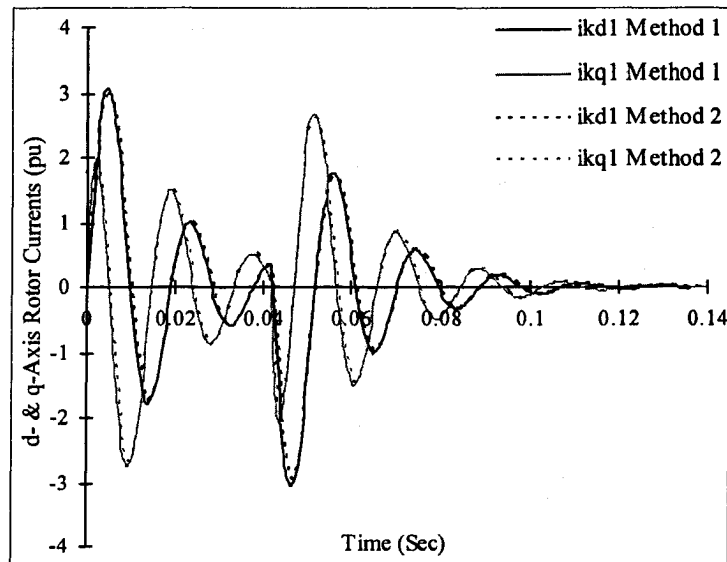


Fig. 28. d- and q-axis damper winding currents for generator under lagging power factor condition and short-circuit duration of 41.67 ms.

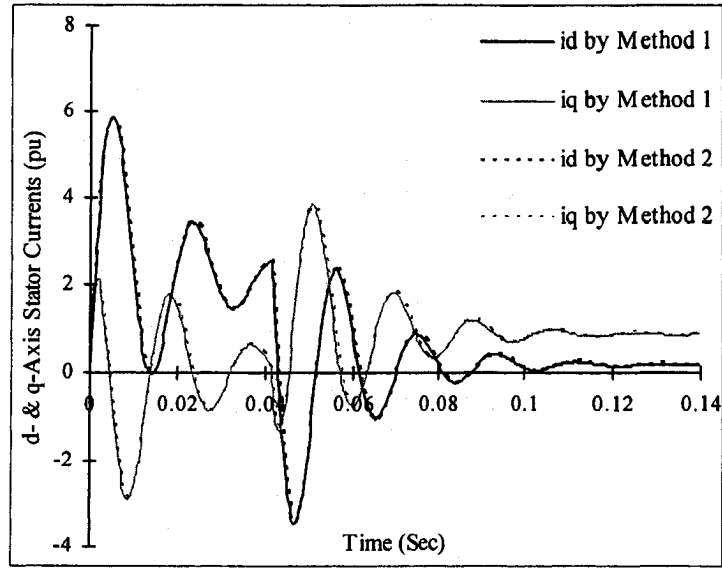


Fig. 29. d- and q-axis stator currents for generator under leading power factor condition and short-circuit duration of 41.67 ms.

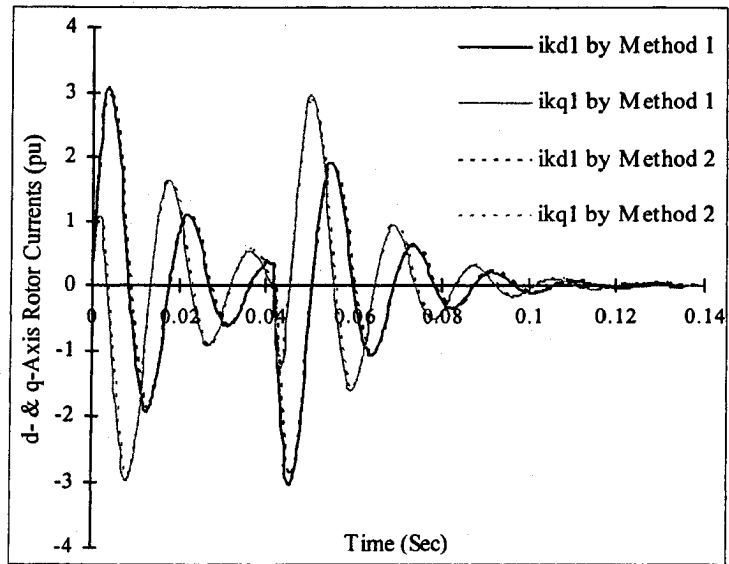


Fig. 30. d- and q-axis damper winding currents for generator under leading power factor condition and short-circuit duration of 41.67 ms.

### 4.3.2 Short-Circuit Analysis

To analyze the effect of three-phase short-circuit fault on the motor transient performance, the developed unsaturated and saturated models have been applied for the same loading conditions mentioned in section 4.1.1 and under lagging power factor condition.

The pre-short-circuit (steady-state) terminal voltage is 1.0 pu and the short-circuit occurred at 12.5 ms (30 time steps) and after a voltage fall duration of 2.5 ms, the terminal voltage becomes zero. Short-circuit continues for two cycles. After the resumption of normal operation, the post-short-circuit terminal voltage comes back to 1.0 pu following a 2.5 ms recovery duration. Figures 31 to 33 show some of the results of these investigations.

The produced air-gap torque and phase 'a' current calculated by considering and ignoring the saturation for fault duration of 33.33 ms are shown in Figs. 31 and 32, respectively. Voltage fall and recovery durations are 2.5 ms each. It can be seen from these figures that there are considerable discrepancies between the results calculated by the model ignoring saturation and the ones calculated by the models that consider saturation. Moreover, as illustrated in these figures, the effect of the inclusion of saturation along the direct axis on the air-gap torque and phase 'a' current is significant.

The dynamic performance of the permanent magnet synchronous motor during and after fault is illustrated in Fig. 33 for different saturation conditions. The amplitude of the load angle swings is relatively smaller in the case of the models that consider saturation. It can be seen from Fig. 33 that the saturation contributes negative damping and higher synchronizing torque (higher frequency of load angle swing) as compared to the ones by the model ignoring saturation. Moreover, there are discrepancies between the results calculated by the models considering saturation.

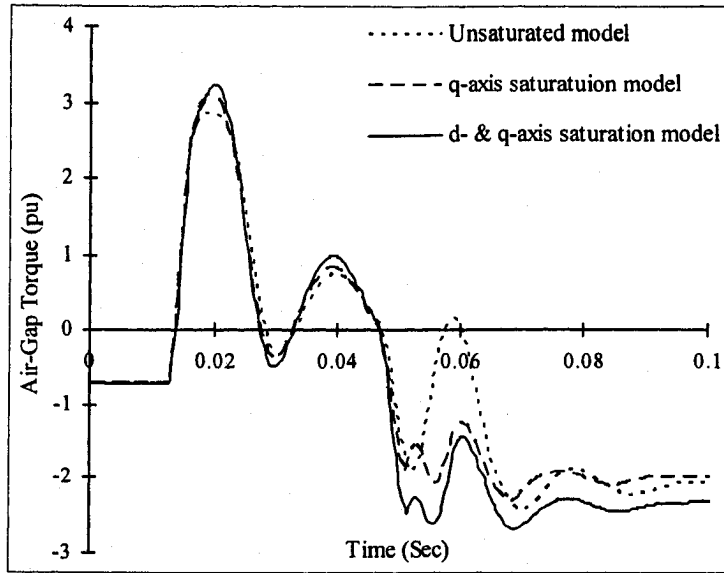


Fig. 31. Air-gap torque by the three saturation models under lagging power condition for short-circuit duration of 33.33 ms and voltage fall/recovery duration of 2.5 ms.

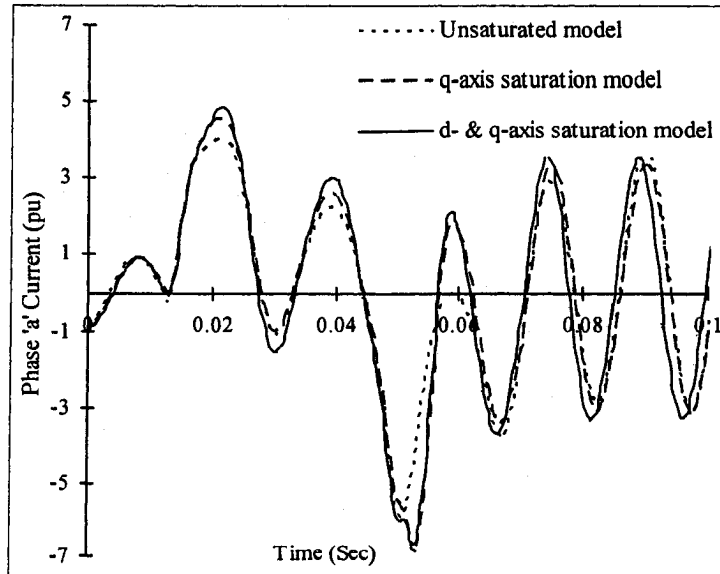


Fig. 32. Phase 'a' current by the three saturation models under lagging power condition for short-circuit duration of 33.33 ms and voltage fall/recovery duration of 2.5 ms.



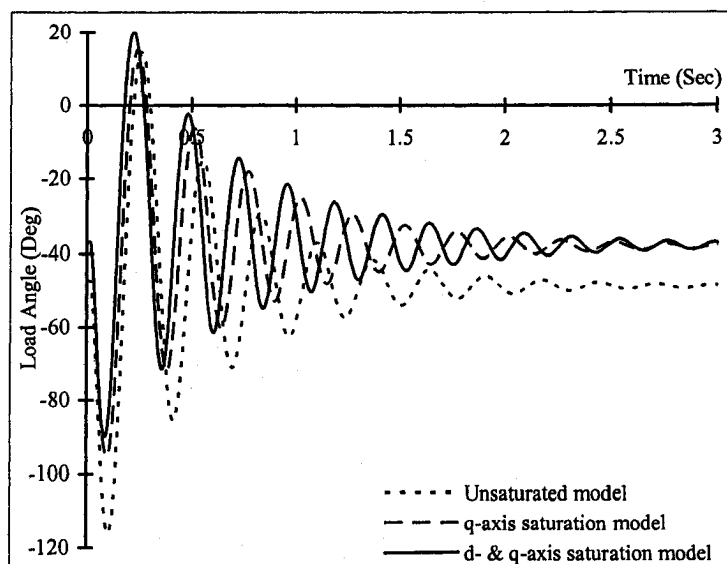


Fig. 33. Load angle by the three saturation models under lagging power condition for short-circuit duration of 33.33 ms and voltage fall/recovery duration of 2.5 ms.

### 4.3.3 Voltage Sag Analysis

To investigate the effect of voltage sag on the transient performance of saturated permanent magnet synchronous motors, the proposed models have been applied to a typical permanent magnet synchronous motor. In the simulations the impact of voltage sag magnitude and duration are investigated. The following are assumed:

- 1) A symmetrical three-phase voltage sag of constant magnitude of 0.2 pu (80% reduction) has been considered.
- 2) Upon voltage restoration, the post-sag terminal voltage comes back to the pre-sag voltage level 1.0 pu while considering a fall/recovery duration of 2.5 ms.
- 3) Voltage sag is initiated at 12.5 ms (30 time steps).

The transient performance has been calculated ignoring and considering the saturation for a loading condition corresponding to active power 0.75 pu and reactive power 0.5 pu under lagging power factor condition at the terminal of the motor. The transient performances of the saturated motor have been determined for voltage fall and recovery durations equal to 2.5 ms. Figures 34 to 41 show some of the results of these investigations.

The produced air-gap torque for the two sag durations (28.33 ms and 38.33 ms) and sag magnitude equal to 0.2 pu are shown in Figs. 34 and 35. As it can be seen from these figures, the post-sag peak air-gap torque has a higher negative magnitude for the sag duration of 38.33 ms in comparison to the one for a sag duration of 28.33 ms. Also, it can be seen that there are discrepancies between the results calculated by the three models.

This negative peak value of the air-gap torque also changes as a function of the sag magnitude as demonstrated in Fig. 36 for the case of the sag duration of 38.33 ms. In this figure it can be seen that there are discrepancies between the results calculated by the three models which show the importance of including both the d- and q-axis saturation in the transient analysis of interior permanent magnet synchronous machines. So, as it can be seen from Figs. 34-36, the effect of the sag magnitude and duration on the post-sag air-gap torque is appreciable. Moreover, there are discrepancies between results calculated by the three models.

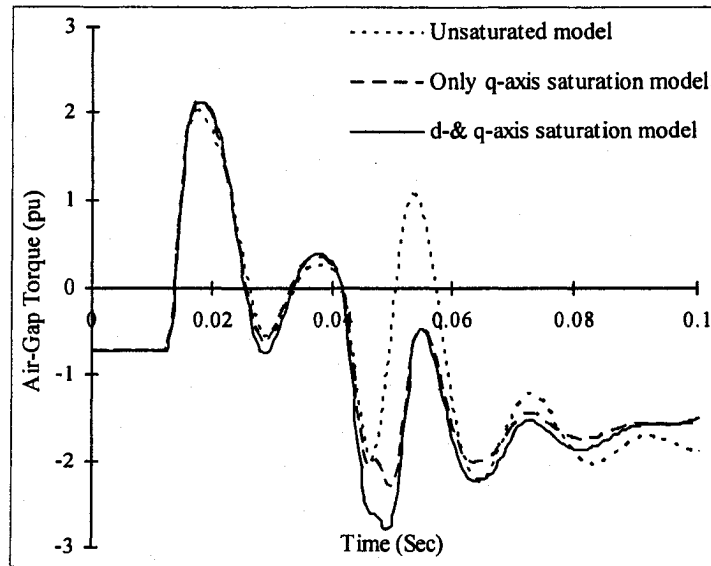


Fig. 34. Motor air-gap torque calculated by various models under lagging power factor condition for sag duration of 28.33 ms.

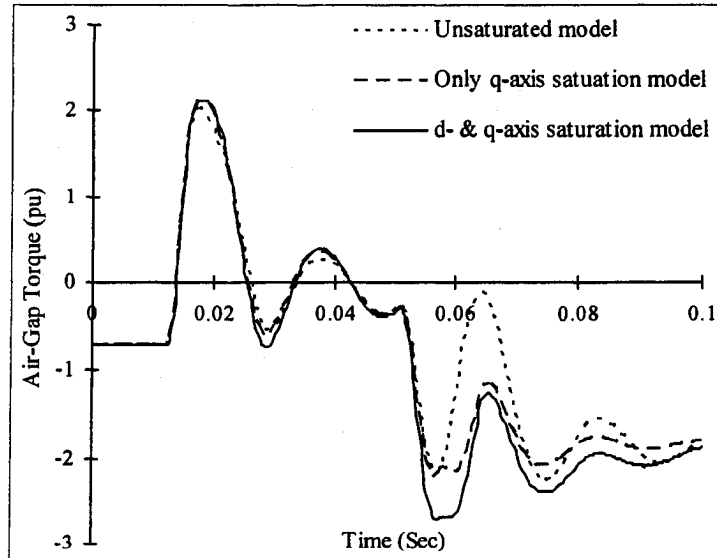


Fig. 35. Motor air-gap torque calculated by various models under lagging power factor condition for sag duration of 38.33 ms.

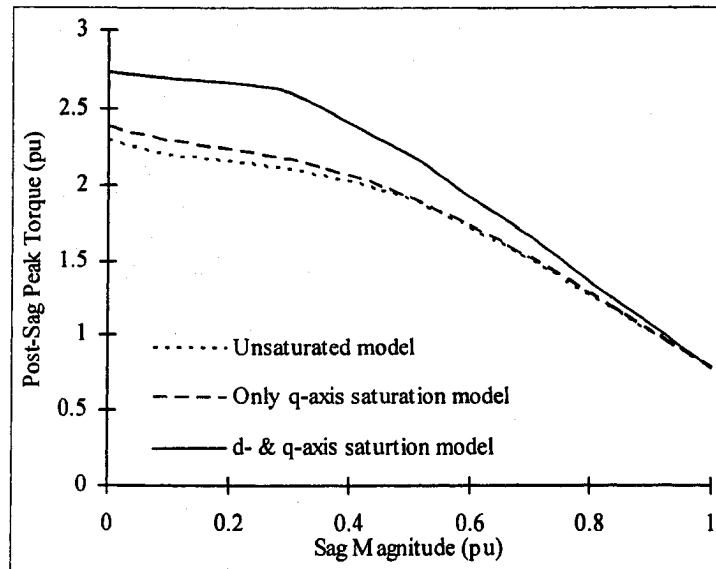


Fig. 36. Peak torque vs sag magnitude calculated by the various models under lagging power factor condition for sag duration of 38.33 ms.

The pattern of the changes of the peaks of the various post-sag phase currents with the sag duration and magnitude is similar to the change of the peaks of the post-sag air-gap torque. For example, the post-sag peak phase 'a' current has a high positive magnitude for the sag duration of 38.33 ms, while it has a relatively smaller value for the sag duration of 28.33 ms as shown in Figs. 37 and 38. The peak value of the phase 'a' current also changes with the sag magnitude as demonstrated in Fig. 39 for the case of the sag duration of 38.33 ms. As can be seen from Figs. 37-39, the effect of the sag magnitude and duration on the post-sag phase 'a' current is appreciable. As well there are noticeable discrepancies between the results calculated by the three saturation models as shown in Figs. 37-39.

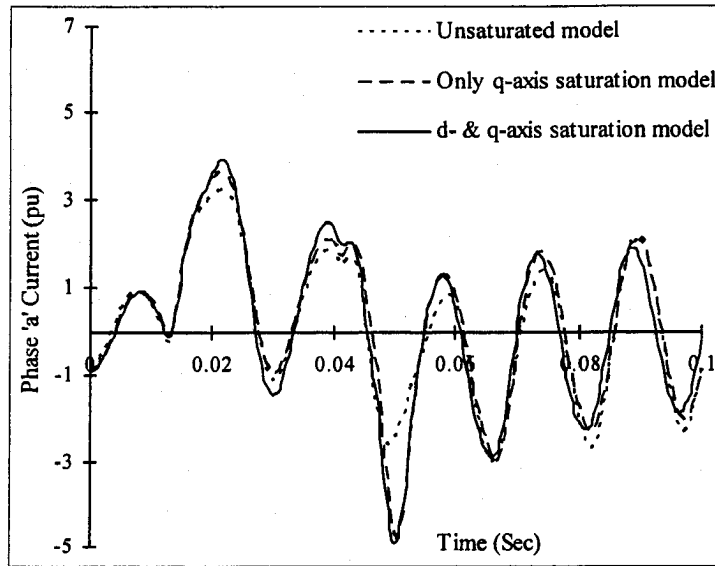


Fig. 37. Motor phase 'a' current calculated by various models under lagging power factor condition for sag duration of 28.33 ms.

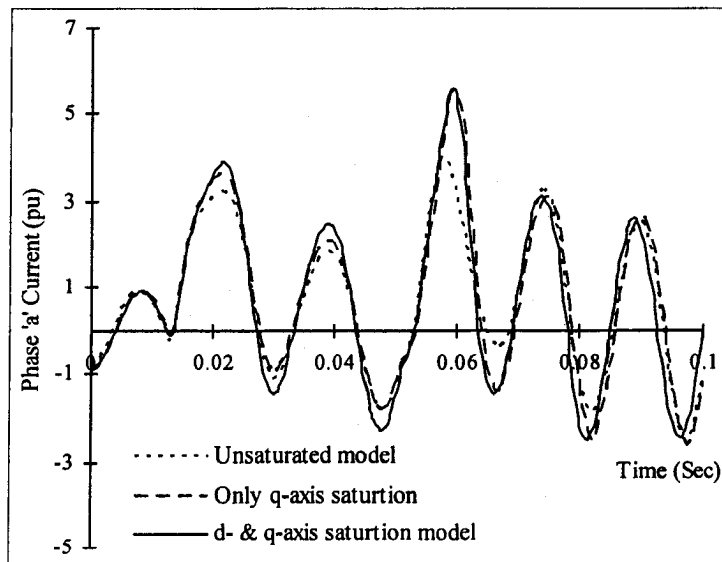


Fig. 38. Motor phase 'a' current calculated by various models under lagging power factor condition for sag duration of 38.33 ms.

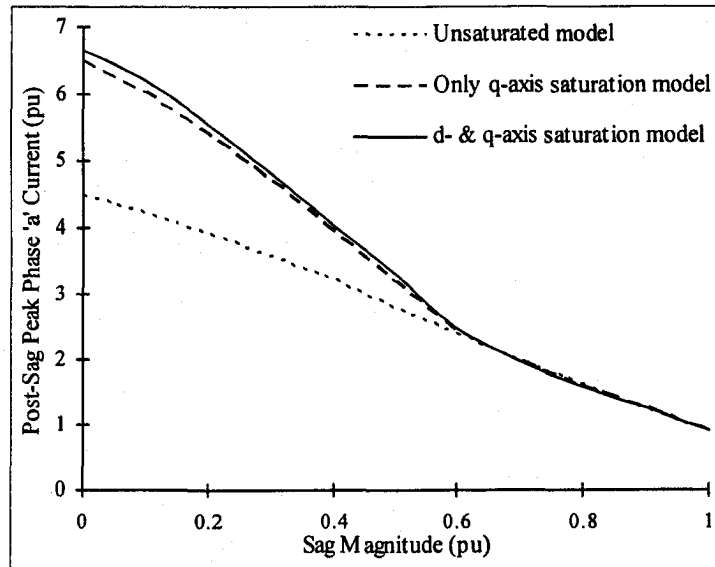


Fig. 39. Motor peak phase 'a' current vs sag duration calculated by the various models under lagging power factor condition for sag duration of 38.33 ms.

The dynamic performance of the permanent magnet synchronous motor during and post-sag durations are illustrated in Figs. 40 and 41 for the two sag durations 28.33 ms and 38.33 ms and sag magnitude of 0.2 pu and a voltage fall and recovery durations of 2.5 ms. As can be seen from these figures, the magnitude and frequency of the load angle swings are relatively higher in the case of the sag duration of 38.33 ms in comparison to the ones for the sag duration of 28.33 ms. It can be seen from Figs. 40 and 41 that the models that consider saturation contribute to more negative damping and higher synchronizing torque (higher frequency of load angle swing) as compared to the ones by the model ignoring saturation. Among the two saturation models, the model considering saturation in both d- and q-axis introduces the more negative damping and the higher synchronizing torque.

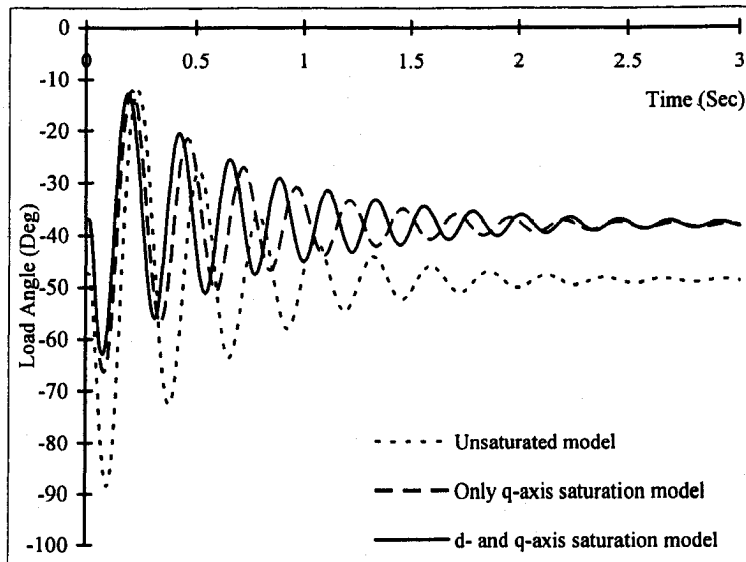


Fig. 40. Motor Load Angle calculated by various models under lagging power factor condition for sag duration of 28.33 ms.

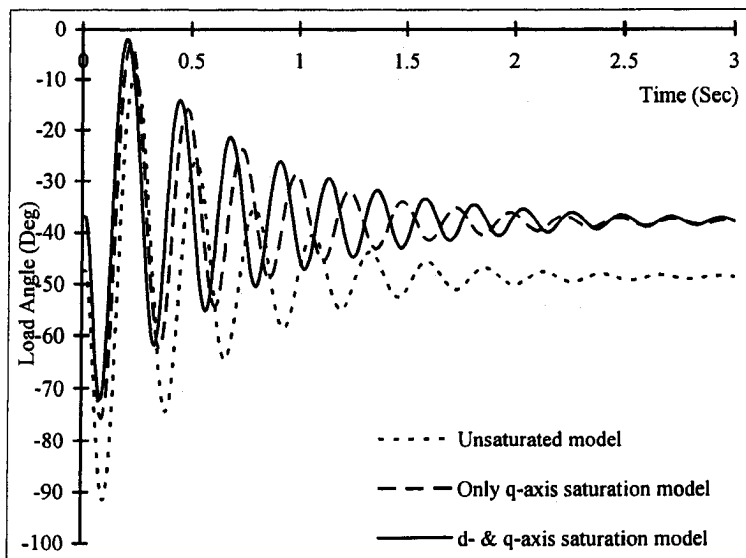


Fig. 41. Motor Load Angle calculated by various models under lagging power factor condition for sag duration of 38.33 ms.

#### 4.3.4 Voltage Swell Analysis

In the analysis of the transient performance of permanent magnet synchronous motors during and after the swell, the accurate calculation of the stator and rotor currents, load angle and air-gap torque depends on the saturation conditions. So to investigate the effect of voltage swells on the transient performances of saturated permanent magnet synchronous motors, the proposed models have applied to a typical permanent magnet synchronous motor. In these investigations, the following are assumed:

1. A symmetrical three-phase voltage swell of magnitude 1.5 pu has been considered.
2. Upon voltage restoration, the post-swell terminal voltage comes back to the pre-swell voltage level 1.0 pu while considering a fall/recovery duration of 2.5 ms.
3. Voltage swell is initiated at 12.5 ms (30 time steps).

The transient performance has been calculated considering and ignoring the saturation for a loading condition corresponding to real power = 0.75 pu and reactive power = 0.5 pu under lagging power factor condition at the terminal of the motor. The pre-swell terminal voltage  $V_t$  is 1.0 pu and the terminal voltage amplitude increases to 150% (1.5 pu) of the pre-swell voltage at 12.5 ms and the voltage swell continues for either 28.33 ms or 38.33 ms and voltage fall and recovery durations are 2.5 ms each. After the resumption of normal operation, the post-swell terminal voltage comes back to 1.0 pu. Figures 42 to 50 show some of the results of these investigations.

The proposed air-gap torque for the two 28.33 ms and 38.33 ms swell durations are shown in Figs. 42 and 43. As can be seen from these figures, the peak values of the post-swell air-gap torque have larger positive magnitudes for the swell duration of 28.33 ms in



comparison to the one for a swell duration of 38.33. Moreover, The largest positive peak values of the post-swell air-gap torque also change as a function of the swell magnitude as demonstrated in Fig. 44 for the case of a swell duration of 38.33 ms. As it can be seen from Figs. 42 to 44 the effect of the swell magnitude and duration on the post-swell air-gap torque is appreciable. Also, the saturation representation (both d- and q-axis saturation model & only q-axis saturation model) in the permanent magnet synchronous motor modeling can affect the accuracy of calculating this torque.

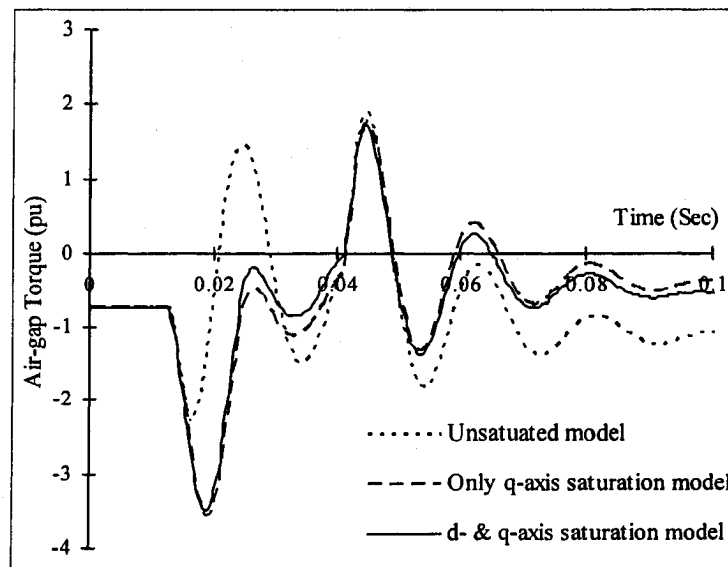


Fig. 42. Motor air-gap torque calculated by the various models under lagging power factor condition for voltage swell duration of 28.33 ms.

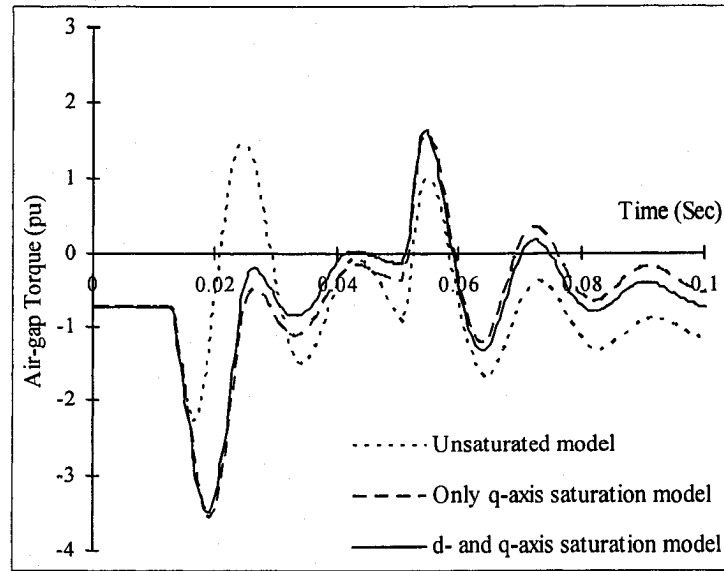


Fig. 43. Motor air-gap torque calculated by the various models under lagging power factor condition for voltage swell duration of 38.33 ms.

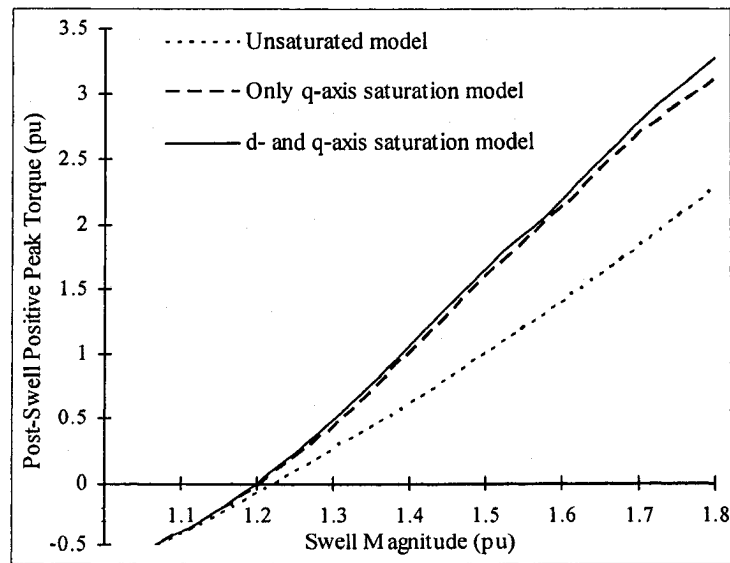


Fig. 44. Largest positive peak value of the post-swell air-gap torque vs swell magnitude calculated by the various models under lagging power factor condition for voltage swell duration of 38.33 ms.

The changes of the peaks of the post-swell phase currents depend also on the swell duration and magnitude. For example, the peaks of the post-swell phase 'a' current have larger positive magnitudes for the swell duration of 28.33 ms in comparison to the one for a swell duration of 38.33 ms as shown in Figs. 45 and 46. It can also be Fig. 47 that the change of the largest negative peak value of the phase 'a' current changes with the swell magnitude for the case of a swell duration of 28.33 ms. So, as it can be seen from Figs. 45-47, the effect of the swell magnitude and duration on the post-swell phase 'a' current is appreciable. Also it is noticeable from Figs. 45-47 that there are discrepancies between the results calculated by the three saturation models.

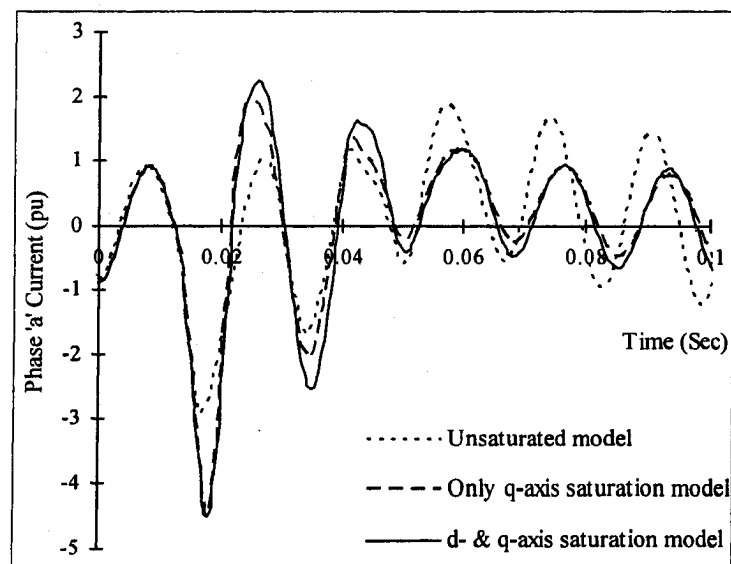


Fig. 45. Motor phase 'a' current calculated by the various models under lagging power factor condition for voltage swell duration of 28.33 ms.

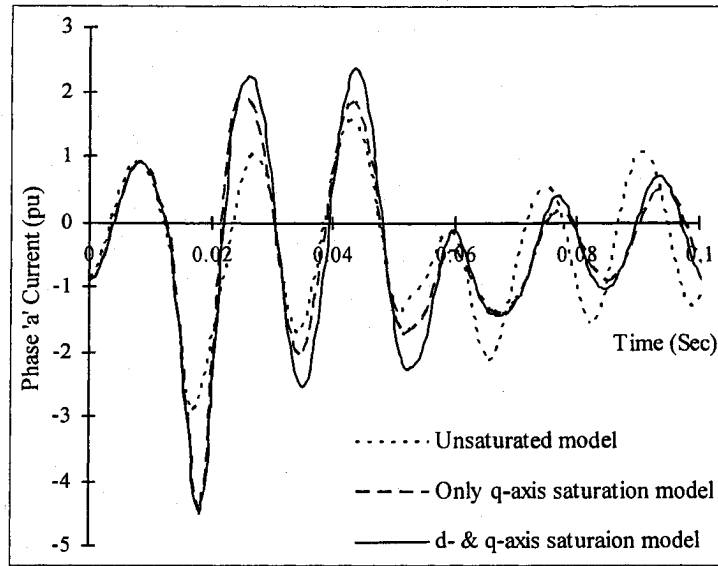


Fig. 46. Motor phase 'a' current calculated by the various models under lagging power factor condition for voltage swell duration of 38.33 ms.

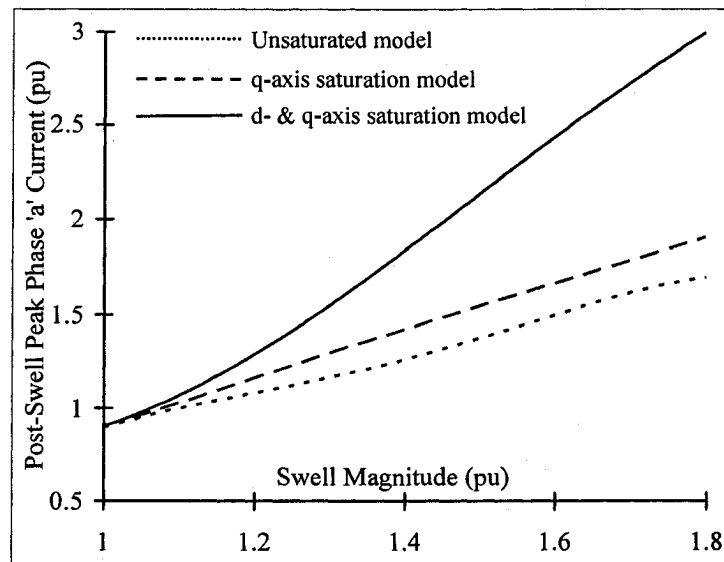


Fig. 47. Largest negative peak value of the post-swell phase 'a' current as a function of the swell magnitude calculated by the various models under lagging power factor condition for voltage swell duration of 28.33 ms.

The dynamic performance of the permanent magnet synchronous motor as affected by the voltage swell and the saturation modelling, is illustrated in Figs. 48 and 49 for the two swell durations 28.33 ms and 38.33 ms and a swell magnitude of 1.5 pu and voltage fall and recovery durations of 2.5 ms. As can be seen from these figures, the amplitude of the load angle swings is dependent on the swell duration. For example, this amplitude of the load angle swings is relatively larger in the case of 38.33 ms swell duration. The saturation representation in the motor modeling can also affect the damping and the frequency of the load angle swings as shown in Figs. 48 and 49. For example, the models that consider saturation contribute to more negative damping and larger synchronizing torque (higher frequency of the load angle swing) as compared to the ones by the model ignoring saturation for both the 28.33 ms and 38.33 ms swell durations.

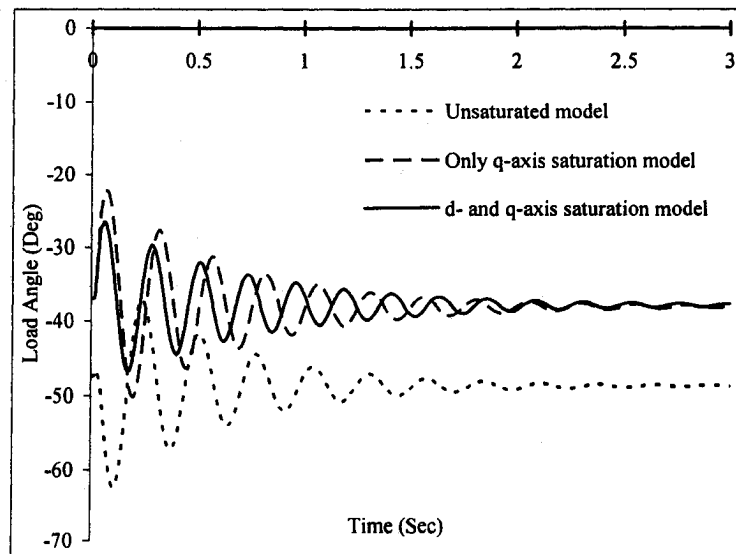


Fig. 48. Motor load angle calculated by the various models under lagging power factor condition for voltage swell duration of 28.33 ms.

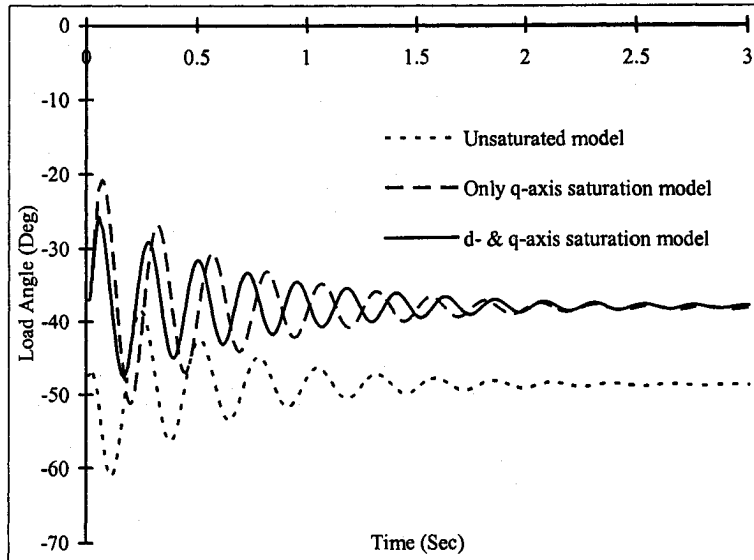


Fig. 49. Motor load angle calculated by the various models under lagging power factor condition for voltage swell duration of 38.33 ms.

#### 4.3.5 Voltage Profile Analysis

As mentioned in the introduction, during the occurrence and clearing of a fault, the machine terminal voltage does not change instantly but rather it takes some time to reach fault value or a post-fault value. The reactive elements of the system, in their effort to prevent instantaneous change in voltage due to the presence of capacitors and instantaneous change in current due to the presence of inductors, establish voltage fall and recovery durations of the pulse waveform that has been shown in Figs. 9(a-c). However, the effect of the voltage fall and recovery durations on the machine performances has not been demonstrated in the literatures. In this section, the following are assumed:

1. A three-phase short-circuit at the motor terminals has been considered.
2. Upon voltage restoration, the post-SC terminal voltage comes back to the pre-SC voltage level 1.0 pu while considering the delay fall/recovery duration of 2.5 ms.
3. Short-circuit is initiated at 12.5 ms (30 time steps).

The most commonly used short-circuit voltage profile has been illustrated in Fig. 9(d). The short-circuit voltage profile which will be used in the investigations of this research work is illustrated in Fig. 50. As can be seen from Fig.50 different voltage fall and recovery durations will be considered to demonstrate their effect on the motor transient performances. In this figure, short-circuit duration of 2 cycles (for a power system frequency of 60 Hz) has been considered. Transient results have been calculated considering and ignoring the saturation for a loading condition corresponding to real power = 0.75 pu and reactive power = 0.5 pu under lagging power factor condition at the terminals of the motor.

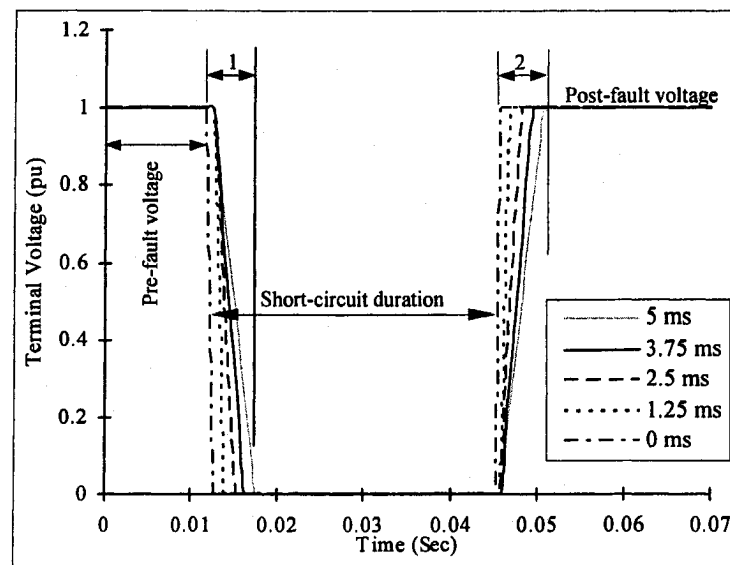


Fig. 50. Proposed voltage profile due to short-circuit at the motor terminals with different voltage fall and recovery durations.

- |    |   |
|----|---|
| 1. | Voltage fall duration from steady-state value to zero value             |
| 2. | Voltage recovery duration from zero value to a post-short-circuit value |
| 3. | Short-circuit duration  |

The effect of voltage fall/recovery durations on the motor air-gap torque and the phase 'a' current is illustrated in Figs. 51 and 52, respectively. It is noticeable from these figures that the motor transient performances are highly dependent on the durations of voltage fall and voltage recovery. The oscillations in the air-gap torque and phase 'a' current are the highest if the terminal voltage falls to zero value immediately and recovers to the post-short-circuit value immediately. On the other hand, as it might be expected, the oscillations in the air-gap torque and phase 'a' current reduce significantly with the consideration of the voltage fall/recovery time. The effects of the saturation modeling and the voltage fall/recovery durations on the motor load angle are illustrated in Fig. 53. As can be seen from this figure, the load angle swing reduces with the increase of the voltage fall/recovery duration and the effect of voltage fall/recovery duration on the load angle swing becomes less if saturation is considered in the machine modeling.

The effects of the saturation modeling and the voltage fall/recovery duration on the motor critical clearing time are illustrated in Fig. 54. As can be seen from this figure, the motor critical clearing time increases with the increase of the voltage fall/recovery durations and the effect of the inclusion of saturation in the motor modeling is also to increase the critical clearing time.



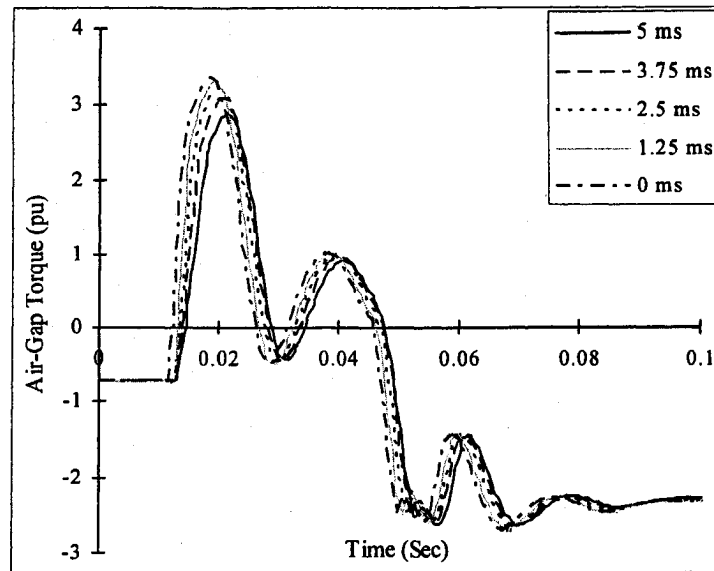


Fig. 51. Air-gap torque calculated using model considering both d- and q-axis saturation for short-circuit duration of 33.33 ms and using voltage fall and recovery duration of 0, 1.25, 2.5, 3.75 and 5 ms each.

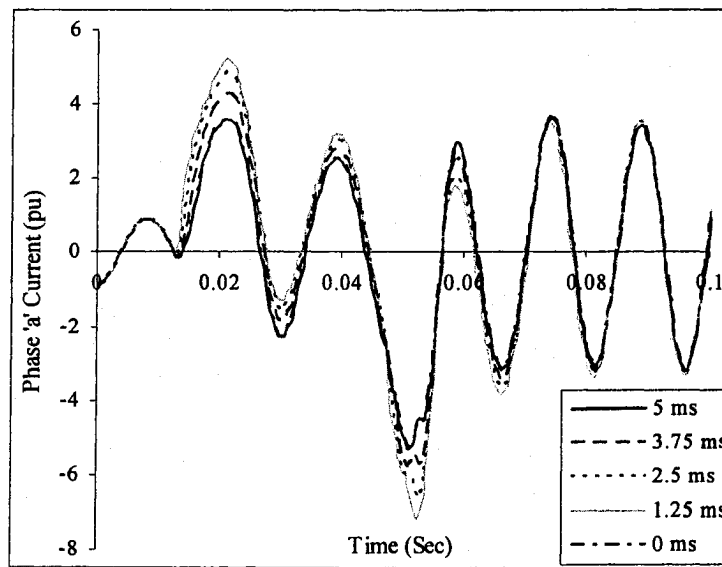


Fig. 52. Phase 'a' current calculated using model considering both d- and q-axis saturation for short-circuit duration of 33.33 ms and using voltage fall and recovery duration of 0, 1.25, 2.5, 3.75 and 5 ms each.

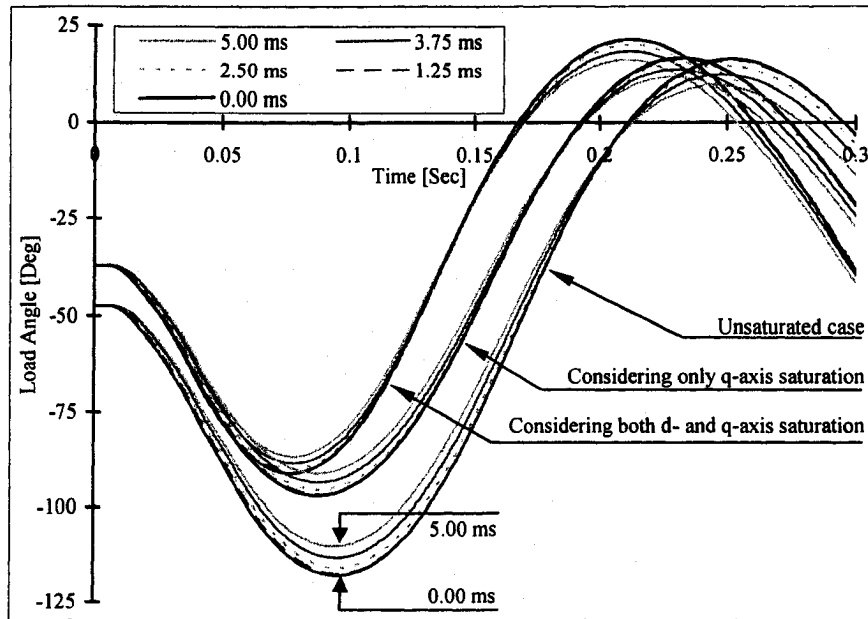


Fig. 53. Load angle calculated using the three saturation models for short-circuit duration of 33.33 ms and using voltage fall and recovery duration of 0, 1.25, 2.5, 3.75 and 5 ms each.

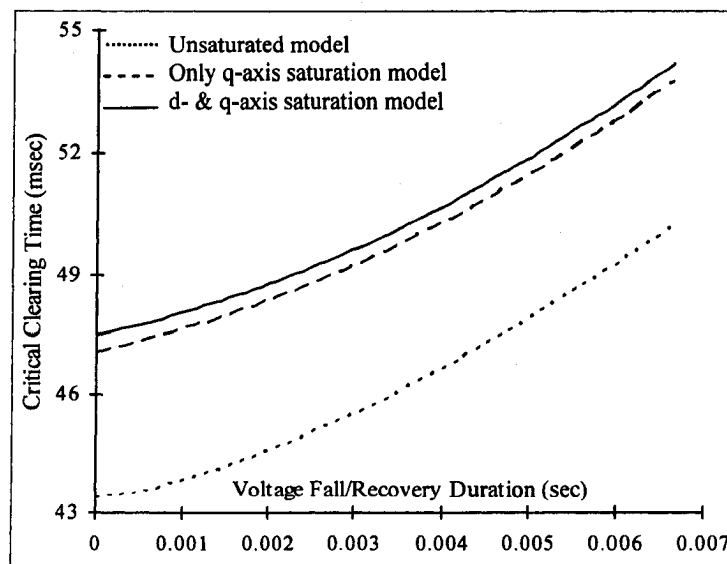


Fig. 54. Motor critical clearing time as a function of voltage fall/recovery duration calculated by the three saturation models.

## 5. Conclusion

This research work is an attempt to develop mathematical models of interior permanent magnet synchronous machine considering machine magnetic parameter variations due to saturation to predict the machine transient performance accurately. The following conclusions can be made from the finding of these investigations:

1. The flux differential equations method and the current differential equations method give the same results. So modeling the permanent magnet synchronous machines using either of these methods will produce the same result.
2. The use of the unsaturated values of the d- and q-axis magnetizing reactances can lead to significant errors in the machine transient performance predictions.
3. There are noticeable discrepancies between the results of the air-gap torque, load angle and the current values calculated by the models considering saturation and those calculated by the model ignoring saturation.
4. The effect of inclusion of d-axis saturation on the motor transient performance is significant.
5. Saturation contributes negative damping and results in an increased frequency of the load angle swings.
6. Deeper voltage sags generally cause larger torque peaks.
7. Deeper voltage sags generally cause higher current peaks.
8. The effect of the voltage sag magnitude and duration on the transient performance of saturated permanent magnet synchronous motor is extremely large.
9. The effect of the voltage swell magnitude and duration on the transient performance of saturated permanent magnet synchronous motors is large.

10. There are also discrepancies between the results of the air-gap torque and the stator current calculated by saturation models and unsaturated model.
11. The dynamic performance (the load angle swing) is dependent on the swell duration and the saturation representation in the permanent magnet synchronous motors modeling.
12. The damping and the frequency of the load angle swings are dependent on the saturation representation in the permanent magnet synchronous motors modeling.
13. The effect of the voltage fall/recovery duration on the transient performance of saturated permanent-magnet synchronous motor is significant.
14. The amplitudes of the motor transient oscillations reduce with the increase in the voltage fall/recovery duration.
15. Critical clearing time increases with the increase of the voltage fall/recovery duration and with the inclusion of saturation in the motor modeling.

## References

- [1] H. Wijenayake and P. B. Schmidt, "Modeling and Analysis of Permanent Magnet Synchronous Motor by Taking Saturation and Core Loss into Account", in *Proc. 1997 IEEE Power Electronics and Drive Systems Int. Conf.*, Vol. 2, pp.530-540.
- [2] Farouk M. Abdel-Kader and Shaban M. Osheba, "Performance Analysis of Permanent Magnet Synchronous Motors. Part I: Dynamic Performance," *IEEE Trans. on Energy Conversion*, Vol. 5, pp. 366-373, 1990.
- [3] P. H. Mellor, M. A. Al-Tae, and K. J. Binns, "Open Loop Stability Characteristics of Synchronous Drive Incorporating High Field Permanent Magnet Motor," in *Proc. of the 1991 IEE*, Vol. 138, No. 4, pp. 175-184, July.
- [4] P. H. Mellor, F. B. Chaaban and K. J. Binns, "Estimation of Parameters and Performance of Rare-Earth Permanent-Magnet Motors Avoiding Measurement of Load Angle," in *Proc. of 1991 IEE*, Vol. 138, No. 6, pp. 322-330, November.
- [5] K. J. Binns, and T. M. Wong, "Analysis and Performance of Permanent Magnet Synchronous Machine," in *Proc. of the 1984 IEE*, Vol. 131, No. 6, pp. 252-257.
- [6] P. Vas and W. Drury, "Future of Electrical Machines and Drives," in *Proc. of the 1996 Int. Conf. on Electrical Machines*, Vol. 3, Vigo, Spain, pp. 67-74.
- [7] Tim Miller, "Brushless Permanent-Magnet Motor Drives," *Power Engineering Journal*, Vol. 2, Issue 1, pp. 55-60, January 1988.
- [8] M. Azizur Rahman and Ping Zhou, "Analysis of Brushless Permanent Magnet Synchronous Motors," *IEEE Trans. on Industrial Electronics*, Vol. 43, No. 2, pp. 256-267, April 1996.
- [9] T. Sebastian and G. R. Slemon, "Operating Limits of Inverter-Driven Permanent Motor Drives," *IEEE Trans. on Industry Applications*, Vol. IA-23, No. 2, pp. 327-333, 1987.
- [10] K. J. Binns, M. A. Jabbar, and W. R. Barnard, "Hybrid Permanent Magnet Synchronous Motors," in *Proc. of the 1978 IEE*, Vol. 125, No. 3, pp. 203-207.
- [11] Pragasan Pillay and R. Krishnan, "Modeling of Permanent Magnet Motor Drives," *IEEE Trans.s on Industrial Electronics*, Vol. 35, No. 4, pp. 537-541, November 1988.

- [12] P. Krause, *Analysis of Electric Machinery*, New York: McGraw Hill: 1986.
- [13] Stephen J. Chapman, *Electric Machinery Fundamentals*, Third Edition: *McGraw-Hill*; 1999.
- [14] D.W. Shimmin, J. Wang, N. Bennett, and K.J. Binns, "Modeling and Stability Analysis of a Permanent-Magnet Synchronous Machine Taking into Account the Effect of Cage Bars," in *Proc. of the 1995 IEE Electric Power Application*, Vol. 142, No.2, pp. 137-144, March.
- [15] P. Pillay and R. Krishnan, "Modeling, Simulation, and Analysis of Permanent-Magnet Motor Drives, Part I: The Permanent-Magnet Motor Drive," *IEEE Trans. on Industry Applications*, Vol. 25, No. 2, pp. 265-273, 1989.
- [16] E. C. Lovelace, T. M. Jahns, and J. H. Lang, "Impact of Saturation and Inverter Cost on Interior PM Synchronous Machine Drive Optimization," *IEEE Trans. on Industry applications*, Vol. 36, Issue 3, pp. 723-729, 2000.
- [17] A. Fratta, A. Vagati, and F. Villata, "Design Criteria of an IPM Machine Suitable for Field-Weakened Operation," in *Proc. of the 1990 Int. Conf. of the Electrical Machines*, pp. 1059-1065.
- [18] N. Urasaki, T. Senjyu, and K. Uezato, "Relationship of Parallel Model and Series Model for PMSM Including Iron Loss," *32<sup>nd</sup> Annual 2001 IEEE Power Electronics Specialists Conference*, Vol. 2, pp. 788-793, 17-21 June.
- [19] B. Stumberger, G. Stumberger, D. Dolinar, A. Hamler, and M. Trlep, "Evaluation of Saturation and Cross-Magnetization Effects in Interior Permanent-Magnet Synchronous Motor," *IEEE Trans. on Industry Applications*, Vol. 39, No. 5, pp. 1264-1271, September/October 2003.
- [20] T. A. Lipo, T. J. E. Miller, A. Vagati, L. Malesani, and T. Fukao, "Synchronous Reluctance Drives Tutorial," in *Proc. of the 1994 IEEE IAS Annual Meeting*.
- [21] A. Vagati, A. Fratta, G. Franceschini, and P. M. Rosso, "A.C. Motors for High-Performance Drives: A Design-Based Comparison," in *Proc. of the 1995 IEEE IAS Annual Meeting*, pp. 725-733.
- [22] E. C. Lovelace, T. M. Hahns, and J. H. Lang, "A Saturating Lumped-Parameter Model for an Interior PM Synchronous Machine," *IEEE Trans. on Industry Applications*, Vol. 38, pp.645-650, 2002.

- [23] E. C. Lovelace, T. Keim, J. H. Lang, D. D. Wentzloff, T. M. Jahns, J. Wai, and P. J. McCleer, "Design and Experimental Verification of a Direct-Drive Interior PM Synchronous Machine Using a Saturable Lumped-Parameter Model," in *Proc. of the 2002 IEEE Industry Applications Conference*, Vol. 4, pp. 2486-2492.
- [24] Alfio Consoli, and Agnelo Raciti, "Analysis of Permanent Magnet Synchronous Motors," *IEEE Trans. on Industry Applications*, Vol. 27, No. 2, pp. 350-354, March/April 1991.
- [25] M. A. Rahman and A. M. Osheiba, "Performance of Large Line-Start Permanent Magnet Synchronous Motors," *IEEE Trans. on Energy Conversion*, Vol. 5, No. 1, pp. 211-217, March 1990.
- [26] C. Mademlis and V. G. Agelidis, "On Considering Magnetic Saturation with Maximum Torque to Current Control in Interior Permanent Magnet Synchronous Motor Drives," *IEEE Trans. on Energy Conversion*, Vol. 16, No. 3, pp. 246-252, September 2001.
- [27] X. Luo and T. A. Lipo, "A Synchronous/Permanent Magnet Hybrid AC Machine," *IEEE Trans. on Energy Conversion*, Vol. 15, No. 2, pp. 203-210, June 2000.
- [28] S.A. Nasar, I. Bodea, and L.E. Unnewehr, "Permanent Magnet, Reluctance, and Self-Synchronous Motors," *Florida: CRC Press, Inc.*, 1993.
- [29] *IEEE Recommended Practice for Monitoring Electric Power Quality*, IEEE Standards Board, pp. 5, June 14, 1995.
- [30] V. B. Honsinger, "Performance of Polyphase Permanent Magnet Machines," *IEEE Transaction on Power Apparatus and System*, Vol. PAS-99, No. 4, pp. 1510-1518, 1980.
- [31] K. J. Binns, W. R. Barnard, and M. A. Jabbar, "Hybrid Permanent Magnet Synchronous Motors," in *Proceedings of the 1978 IEE*, Vol. 125, No. 3, pp. 203-207.
- [32] V. B. Honsinger, "The Field and Parameters of Interior Type AC Permanent Magnet Machines," *IEEE Trans. on Power Apparatus and System*, Vol. 101, pp. 867-876, 1982.

- [33] K. J. Binns, and M. A. Jabbar, "High Field Self Starting Permanent Magnet Synchronous Motor", in *Proceedings of the 1981 IEE*, Vol. 128, No. 3, pp. 157-160.
- [34] K. Miyashita, S. Yanshita, S. Tanbe, T. Shimozu and H. Sento, "Developed of a High Speed 2-Pole Permanent Magnet Synchronous Motor," *IEEE Trans. on Power Apparatus and Systems*, Vol. PAS-99, No. 6, pp. 2175-2183, 1980.
- [35] F. A. Fouad, T. W. Nebl, and N. A. Demerdash, "Magnetic Field Modeling of Permanent Magnet Type Electronically Operated Synchronous Machines Using Finite Elements," *IEEE Trans. on Power Apparatus and Systems*, Vol. PAS-100, No. 9, pp. 4125-4135, 1981.
- [36] J. D. Glover and M. S. Sarma, *Power System Analysis and Design*, 3<sup>rd</sup> Edition, Thomson Learning, CA, USA, 2002, pp. 320-325.
- [37] M. F. McGranaghan, "Voltage Sags in Industrial Power Systems," *IEEE Trans. on Industry Applications*, Vol. 29, pp. 397-403, 1993.
- [38] M. H. J. Bollen, "IEEE Tutorial on Voltage Sag Analysis," IEEE Press, October 1999.
- [39] J. Arrillaga, M. H. J. Bollen, and N. R. Watson, "Power Quality Following Deregulation," in *Proc. Of the 2000 IEEE*, Vol. 88, pp. 246-261, February.
- [40] F. Carlsson, H. P. Nee, and C. Sadarangani, "Analysis of Peak Torque of Line-Operated Synchronous Machines Subjected to Symmetrical Voltage Sags," in *Proc. of the 2002 IEE Int. Conf. on Power Electronics, Machines and Drives*, pp. 480-485, June.
- [41] M. McGranaghan, "Effects of Voltage Sags in Process Industry Applications," in *Proc. of the 1995 IEEE/KTH Power Tech Conf.*, Stockholm, Sweden, pp. 4-10.
- [42] J. Lamoree, D. Mueller, P. Vinertt, and W. Jones, "Voltage sag analysis case studies," *IEEE Trans. Industry Applications*, Vol. 30, pp. 1083-1089, July/Aug 1994.
- [43] M. H. J. Bollen, "Voltage Sags; Effects, Mitigation and Prediction," *Power Eng. Journal*, Vol. 10, Issue 3, pp. 129-135, June 3, 1996.
- [44] Fredrik Carlsson, "Before And During Voltage Sags," in *2005 IEEE Industry Applications Magazine*, Vol. 11, Issue 2, pp. 39-46, Mar/Apr.



- [45] IEEE Project 1346 Working group, "Electric Power System Compatibility with Industrial Process Equipment, Part 1: Voltage Sags," in *Proc. of the 1994 IEEE Industrial and Commercial Power Systems Tech. Conf.*, pp. 261-266.
- [46] J. C. Das, "Effect of Momentary Voltage Dips on the Operation of Induction and Synchronous Motors," *IEEE Trans. On Industry Applications*, Vol. 26, pp. 711-718, 1990.
- [47] F. Carlsson and J. Engstrom, "Simulation of Ride-Through Possibilities for a Line Operated Synchronous Machine," in *Proc. of the 2000 IEEE International conference on Power System Technology*, Vol. 2, pp. 989-994, December.
- [48] F. Carlsson, "Saturation in Synchronous Machines due to Voltage Sags," in *Proc. of the 2003 IEEE International Conference on Electrical Machines and Drives*, Vol. 31, pp. 1571-1575, June.
- [49] Narayan C. Kar and Ahmed M. El-Serafi, "Effect of Voltage Sag on the Transient Performance of Saturated Synchronous Motors," in *Proc. of the 2006 IEEE Canadian Conf. on Elec. and Comp. Engineering*, pp. 850-855, May.
- [50] C. Radhakrishna, M. Eshwardas, and G. Chebiyam, "Impact of Voltage Sags in Practical Power System Networks", in *2001 IEEE/PES Transmission and Distribution Conference and Exposition*, Vol. 1, pp. 567-572.
- [51] Z. Wang, J. Y. Fan and Y. H. Shao, "Understanding Transients: A Conceptual Interpretation," *IEEE Trans. on Power Systems*, Vol. 12, No. 2, pp. 521-526, May 1997.
- [52] S. S. Chio, J. D. Li and D. M. Vilathgamuwa, "A Generalized Voltage Compensation Strategy for Mitigating the Impacts of Voltage Sags/Swells," *IEEE Trans. on Power Delivery*, vol. 20, pp. 2289-97, 2005.
- [53] C. J. Melhorn, A. Maitra, W. Sunderman, M. Waclawiak, and A. Sundaram, "Distribution System Power Quality Assessment Phase II: Voltage Sag and Interruption Analysis," in *Proc. of the 2005 IEEE IAS Petroleum and Chemical Industry Conference*, pp. 113-120, September.
- [54] S. J. Hauang, C. T. Hsieh, and C. L. Huang, "Application of Morlet Wavelets to Supervise Power System Disturbances," *IEEE Trans. on Power Delivery*, vol. 14, pp. 235-243, 1999.

- [55] F. Carlsson, "Before and During Voltage Sags," in *2005 IEEE Ind. Appl. Magazine*, pp. 39-46, Mar/Apr.
- [56] M. H. J. Bollen, G. Yalcinkaya, G. Hazza, "The Use of Electromagnetic Transient Programs for Voltage Sag Analysis," in *Proc. of the 1998 IEEE 8<sup>th</sup> Int. Conf. on Harmonics and Quality of Power*, Vol. 1, pp. 598-603, 14-16 October.
- [57] Angel Felce, Guillermo Matas, Ysmael Da Silva, "Voltage Sag Analysis and Solution for an Industrial Plant with Embedded Induction Motors," in *2004 IEEE Industry Applications on 39<sup>th</sup> IAS Annual Meeting Conference Record*, Vol. 4, pp. 2573-2578, October.
- [58] M. H. J. Bollen, "The Influence of Motor Reacceleration on Voltage Sags," *IEEE Trans. on Industry Application*, Vol. 31, No. 4, pp. 667-674, July/August 1995.
- [59] J. Wang, N. Bennett, K. J. Binns, and D. W. Shimmin, "Computational and Experimental Determination of Static and Dynamic Parameters For Modeling Permanent magnet Synchronous Machines," in *1993 IEE Electrical Machines and Drives, Sixth International Conference*, No. 376, pp. 289-294, 8-10 September 1993.
- [60] B.J. Chalmers, S.A. Hamed, and G.D. Baines, "Parameters and Performance of a High Field Permanent Magnet Synchronous Motor for Variable Frequency Operation," in *Proc. of the 1985 IEE*, pt. B., Vol. 132, No.3, pp.117-124, May.
- [61] F. Parasiiti and P. Poffet, "A Model for Saturation Effects in High-Field Permanent Magnet Synchronous Motors," *IEEE Trans. on Energy Conversion*, Vol. 4, No. 3, pp. 487-494, September 1989.
- [62] Alfio Consoli and Angelo Raciti, "Analysis of Permanent Magnet Synchronous Motors," *IEEE Trans. on Industry Applications*, Vol. 27, Issue 2, pp. 350-354, March/April 1991.

## VITA AUCTORIS

NAME: Shahram Najafi

YEAR OF BIRTH: 1970

EDUCATION: Bachelor of Science in electrical engineering  
New Mexico State University, USA  
1989-1993

Masters of Science in electrical engineering  
New Mexico State University, USA  
1993-1995

Masters of Applied Science in electrical engineering  
University of Windsor, CANADA  
2005-2006